Cell Reports

Essential roles of RNA cap-proximal ribose methylation in mammalian embryonic development and fertility

Graphical abstract

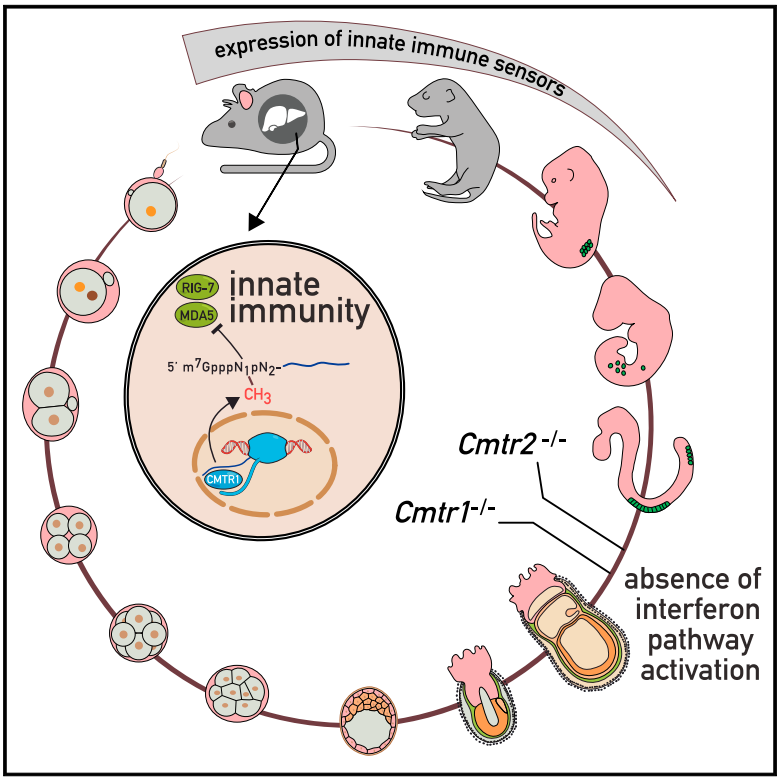

Authors

Michaela Dohnalkova, Kyrylo Krasnykov, Mateusz Mendel, ..., Cathrine Broberg Vågbø, David Homolka, Ramesh S. Pillai

Correspondence

ramesh.pillai@unige.ch

In brief

Mammalian RNA cap-proximal ribose methylations are implicated in preventing the activation of the interferon pathway. Dohnalkova et al. reveal that loss of the mouse RNA methylases CMTR1 and CMTR2 causes embryonic developmental arrest without activation of the interferon pathway, pointing to gene regulatory roles.

Highlights

- CMTR1 and CMTR2 are essential for mouse embryonic development
- Absence of interferon pathway activation in arrested mutant mouse embryos
- Chronic activation of the interferon pathway in *Cmtr1* mutant livers
- Conditional loss of *Cmtr1* in the mouse germline leads to infertility

Dohnalkova et al., 2023, Cell Reports *42*, 112786
July 25, 2023
https://doi.org/10.1016/j.celrep.2023.112786

Cell Reports

CellPress
OPEN ACCESS

Report

Essential roles of RNA cap-proximal ribose methylation in mammalian embryonic development and fertility

Michaela Dohnalkova,[1] Kyrylo Krasnykov,[1] Mateusz Mendel,[1] Lingyun Li,[1] Olesya Panasenko,[2] Fabienne Fleury-Olela,[1] Cathrine Broberg Vågbø,[3] David Homolka,[1] and Ramesh S. Pillai[1,4,*]

[1]Department of Molecular Biology, Science III, University of Geneva, 30 Quai Ernest-Ansermet, 1211 Geneva 4, Switzerland
[2]Department of Microbiology and Molecular Medicine, Faculty of Medicine, University of Geneva, 1 Rue Michel Servet, 1211 Geneva 4, Switzerland
[3]Proteomics and Modomics Experimental Core (PROMEC), Department of Clinical and Molecular Medicine, Norwegian University of Science and Technology (NTNU) and St. Olavs Hospital Central Staff, Trondheim, Norway
[4]Lead contact
*Correspondence: ramesh.pillai@unige.ch
https://doi.org/10.1016/j.celrep.2023.112786

SUMMARY

Eukaryotic RNA pol II transcripts are capped at the 5′ end by the methylated guanosine (m^7G) moiety. In higher eukaryotes, CMTR1 and CMTR2 catalyze cap-proximal ribose methylations on the first (cap1) and second (cap2) nucleotides, respectively. These modifications mark RNAs as "self," blocking the activation of the innate immune response pathway. Here, we show that loss of mouse *Cmtr1* or *Cmtr2* leads to embryonic lethality, with non-overlapping sets of transcripts being misregulated, but without activation of the interferon pathway. In contrast, *Cmtr1* mutant adult mouse livers exhibit chronic activation of the interferon pathway, with multiple interferon-stimulated genes being expressed. Conditional deletion of *Cmtr1* in the germline leads to infertility, while global translation is unaffected in the *Cmtr1* mutant mouse liver and human cells. Thus, mammalian cap1 and cap2 modifications have essential roles in gene regulation beyond their role in helping cellular transcripts to evade the innate immune system.

INTRODUCTION

RNA polymerase II transcripts receive a 5′ methylated guanosine (m^7G) cap that is attached via an inverted 5′–5′ triphosphate linkage to the transcription start site (TSS) nucleotide.[1–7] The m^7G cap is required for translation[8] and RNA stability.[9] This minimal cap structure termed cap0 (m^7GpppN, where N is the TSS nucleotide) is found in lower eukaryotes like yeast. In higher organisms, the TSS nucleotide is 2′-*O*-methylated on the ribose by CMTR1 to create the cap1 structure ($m^7GpppNm$),[10] with most of m^7G-capped RNAs having this methylation.[11] Another mammalian ribose methylase CMTR2, modifies the second cap-proximal nucleotide to create the cap2 structure ($m^7GpppNmpNm$),[12] which is found on approximately 50% of polyadenylated RNAs in human cell cultures.[1,4,13] When the TSS nucleotide is an adenosine (which is usually an Am due to cap1 methylation), mammalian PCIF1 catalyzes base methylation (N^6-methyladenosine, m^6A) to create the m^6Am mark[11] (Figure 1A).

Cap-proximal ribose methylations prevent cellular RNAs from activating the innate immune response pathway.[14] Vertebrate cells have a system of cytosolic sensor proteins[15,16] that recognize molecular features on bacterial and viral nucleic acids to trigger production of secreted cytokines like interferons.[17] The interferons in turn initiate the production of a large set of interferon-stimulated genes (ISGs) in the infected cell and those nearby to create an anti-pathogenic environment.[18] Cap0 is one such "non-self" molecular feature that is recognized by the host innate immune sensors like RIG-I[19] and MDA5.[20] The presence of cap-proximal ribose methylations on RNA substrates reduces binding and, as a consequence, interferon pathway activation, as the methyl group clashes with a conserved histidine (H830) in RIG-I.[21–23] Cap-proximal ribose methylations also protect cellular mRNAs from the negative effects of ISGs like IFIT1 (interferon-induced protein with tetratricopeptide repeats 1), which is a potent translation repressor that binds cap0 RNAs.[24–26] First- or second-position methylation alone can individually reduce binding of IFIT1 to the capped RNA, but cap2 (both first- and second-position methylations) has the strongest inhibitory effect.[24] Consistently, knockdown of host *CMTR1* in mammalian cells triggers expression of ISGs, presumably because of the unmethylated cellular cap0 RNAs being sensed as "non-self."[21,27] Similarly, transfected RNAs with a second-position ribose methylation are identified as "self."[28] In line with this, *CMTR2* KO human HEK293T cells show mild activation of the interferon pathway in an RIG-I-dependent manner.[13] It should be noted that the capacity to sense "non-self" RNAs is not a universal attribute of all cell types.[17]

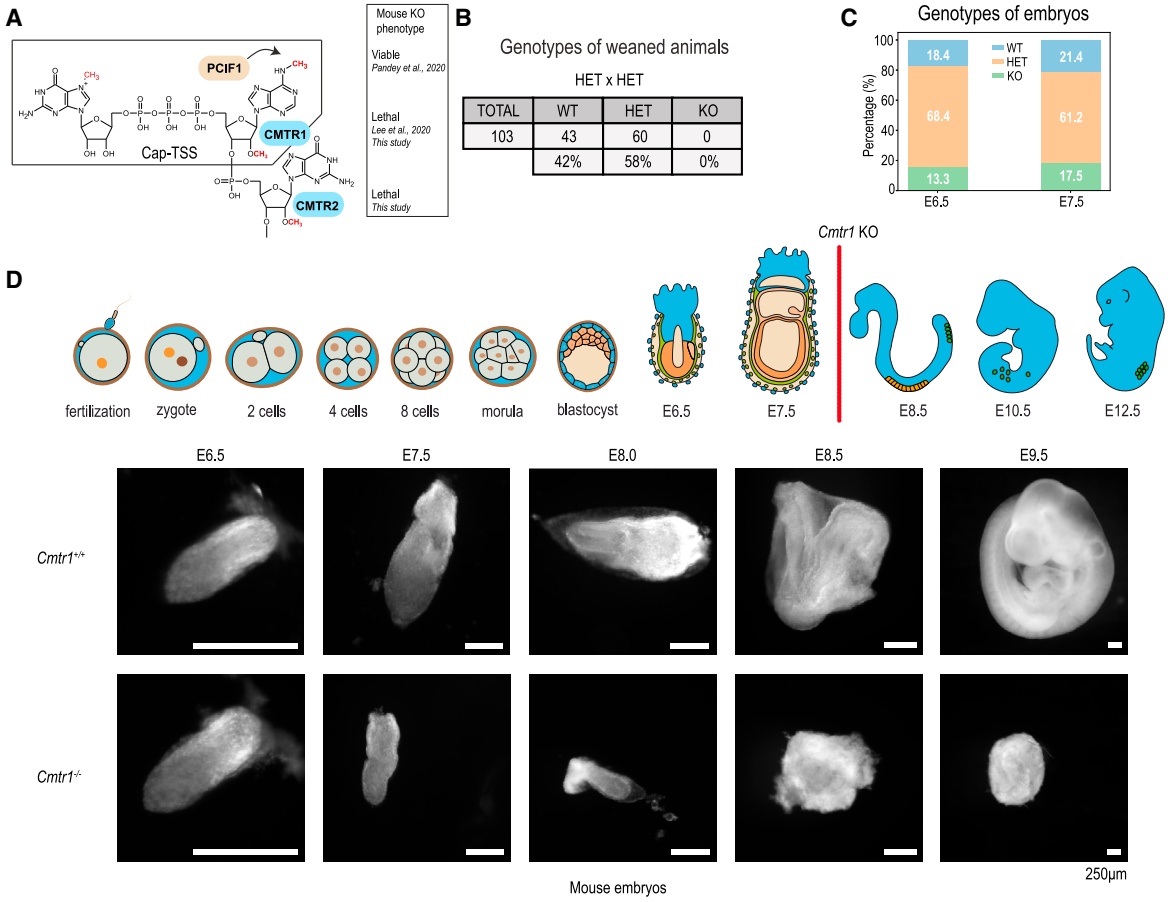

(legend on next page)

Cap-proximal methylations also have a role in cellular gene expression. CMTR1 is nuclear and uses its WW domain to associate with the C-terminal domain (CTD) of RNA pol II.[29] In fact, CMTR1 is found on the TSS of most RNA pol II genes in mouse embryonic stem cells (mESCs) and is required for the transcription of ribosomal protein and histone genes.[30] Knockout of mouse *Cmtr1* leads to embryonic lethality, while conditional deletion in mouse brain affects dendritic morphogenesis.[31] Interestingly, fly Cmtr1 and Cmtr2 act redundantly as the cap1 methylase but act on a distinct set of transcripts, with the double mutant flies showing reward-learning defects.[32] Here, we sought to investigate the tissue-specific roles of CMTR1 and the physiological relevance of CMTR2 using mouse mutants.

RESULTS

Loss of mouse *Cmtr1* leads to embryonic arrest without activating the interferon pathway

To investigate the physiological importance of RNA cap1 methylation (Figure 1A), we examined a *Cmtr1* knockout mouse mutant (STAR Methods and Figure S1A and S1B). Heterozygous *Cmtr1*$^{+/-}$ animals of both sexes are viable and fertile. Crosses between heterozygous individuals resulted in litters that only had wild-type and heterozygous animals at weaning age (Figure 1B), indicating pre-weaning lethality, as previously reported for a gene-trap allele of *Cmtr1*.[31] We isolated embryos at different post-implantation stages and identified them by genotyping (Figure S1C). Homozygous *Cmtr1*−/− embryos (hereafter referred to as the *Cmtr1* mutant) were present at Mendelian ratios at embryonic day 6.5 (E6.5) and E7.5 (Figure 1C), but they were mostly not detected beyond E8.5, with many turning up dead (Figure S1C). The *Cmtr1* mutant embryos are morphologically indistinguishable from the control wild type at E6.5 but are dramatically reduced in size at E7.5, indicating arrested development (Figure 1D).

We sequenced transcriptomes from wild-type and *Cmtr1* mutant embryos at E6.5 and E7.5. Lack of CMTR1 activity is expected to result in host RNA pol II transcripts being unmethylated on the ribose of the first transcribed nucleotide, and such "non-self" cap0 RNAs should normally trigger the interferon pathway.[19–21] Strikingly, there was a complete absence of activation of the interferon pathway genes (Figure 1E and Table S3). Explaining the absence of the interferon pathway activation, a survey of embryonic transcriptomes shows that the different innate immune sensor genes are not expressed in the E6.5 and E7.5 embryos (Figures 1F and S1D). The lethality of *Cmtr1* mouse embryos shows that cap1 RNA methylation has an essential role in early mouse embryonic development, and this is unrelated to its function in preventing activation of the innate immune pathway.

snoRNA host genes are downregulated in the *Cmtr1* mutant embryos

Mouse gastrulation initiates with the formation of the primitive streak at E6.5, through which epiblast cells ingress before being allocated as precursors of the two primary germ layers: the mesoderm and the definitive endoderm.[33] We used the bulk sequencing data to project information on possible cell composition in the embryos (STAR Methods). This reveals a downregulation of gene expression representative of the primitive streak and the mesoderm in the mutant embryos and upregulation of endoderm genes (Figure S1E). Of the over 200 genes altered in the E6.5 mutant embryos, several downregulated genes are those annotated as small nucleolar RNA (snoRNA) host genes (*Snhg12, Snhg8, Snhg5 and Snhg4*) (Figure 1E). Another downregulated gene is the long noncoding RNA *Zfas1*,[34] which is a regulator of epithelial-mesenchymal transition and a snoRNA host gene (for *snord12*). Other downregulated genes include ribosomal protein 20 (Rsp20) and the translation factor eIF4A2, both of which contain intron-encoded snoRNAs. Interestingly, multiple gene copies of the U3 snoRNA (*Rnu3b1*, *Rnu3b3*) show the opposite trend by being upregulated. Unlike the intron-resident snoRNAs, the U3 snoRNA is encoded from an snRNA-type poll II gene that expresses an independent longer precursor form of the RNA.[35]

snoRNAs guide modifications of ribosomal RNAs (rRNAs)[36,37] and spliceosomal small nuclear RNAs (snRNAs).[38] Mammalian snoRNAs are mostly hosted within introns of protein-coding or long noncoding RNAs. Proper splicing and liberation of the introns for further processing of the snoRNA is critical for their biogenesis.[39,40] RNA splicing is influenced by the presence of the m^{7}G cap structure and the proteins that bind it.[41–43] However, quantification of intronic reads from snoRNA host genes did not reveal any striking differences in the *Cmtr1* mutant transcriptomes (Figure S1F). Analysis of global splicing events also did not reveal any dramatic changes in the mutant embryos

Figure 1. Embryonic lethality in the *Cmtr1* mutant mice and downregulation of snoRNA host genes

(A) Chemical structure of the 5′ N^7-methylated guanosine (m^{7}G) cap and cap-proximal ribose methylations. TSS, transcription start site nucleotide. Phenotypes of the mouse knockouts of the enzymes involved are indicated.

(B) Genotypes of animals (at the weaning age) born from heterozygous *Cmtr1* mouse crosses. Numbers of animals (also given as a percentage) are shown. WT, wild type; HET, heterozygous; KO, homozygous knockout. See also Figure S1C.

(C) Genotypes of mouse embryos (shown as percentage) at indicated embryonic days obtained from heterozygous *Cmtr1* mouse crosses.

(D) Cartoon showing mouse embryonic development with the stage at which *Cmtr1* knockout embryos arrest indicated by a red line. Representative wild-type and *Cmtr1* KO embryos at different stages are shown. Notice the degeneration of KO embryos from E8.0 onward.

(E) Volcano plots of differential gene expression between *Cmtr1* KO and wild-type in E6.5 and E7.5 mouse embryos. snoRNA host genes are highlighted in red. Absolute log2 fold change (log2FC) cutoff = 1, adjusted p value (padj) cutoff = 0.05.

(F) Boxplot showing expression of selected innate immune sensors from publicly available transcriptome datasets from different mouse embryonic stages. See also Figure S1D.

(G) Comparison of several alternative splicing (AS) events between wild-type and *Cmtr1* KO E6.5 and E7.5 embryos. Delta percent spliced-in (dPSI) score was computed as a difference between *Cmtr1* KO and wild-type PSI scores per AS event. AF, alternative first exon; SE, skipped exon; A3, alternative 3′ splice site; A5, alternative 5′ splice site; RI, retained intron; AL, alternative last exon; MX, mutual exclusion. Further details are in the STAR Methods. See also Figure S1F.

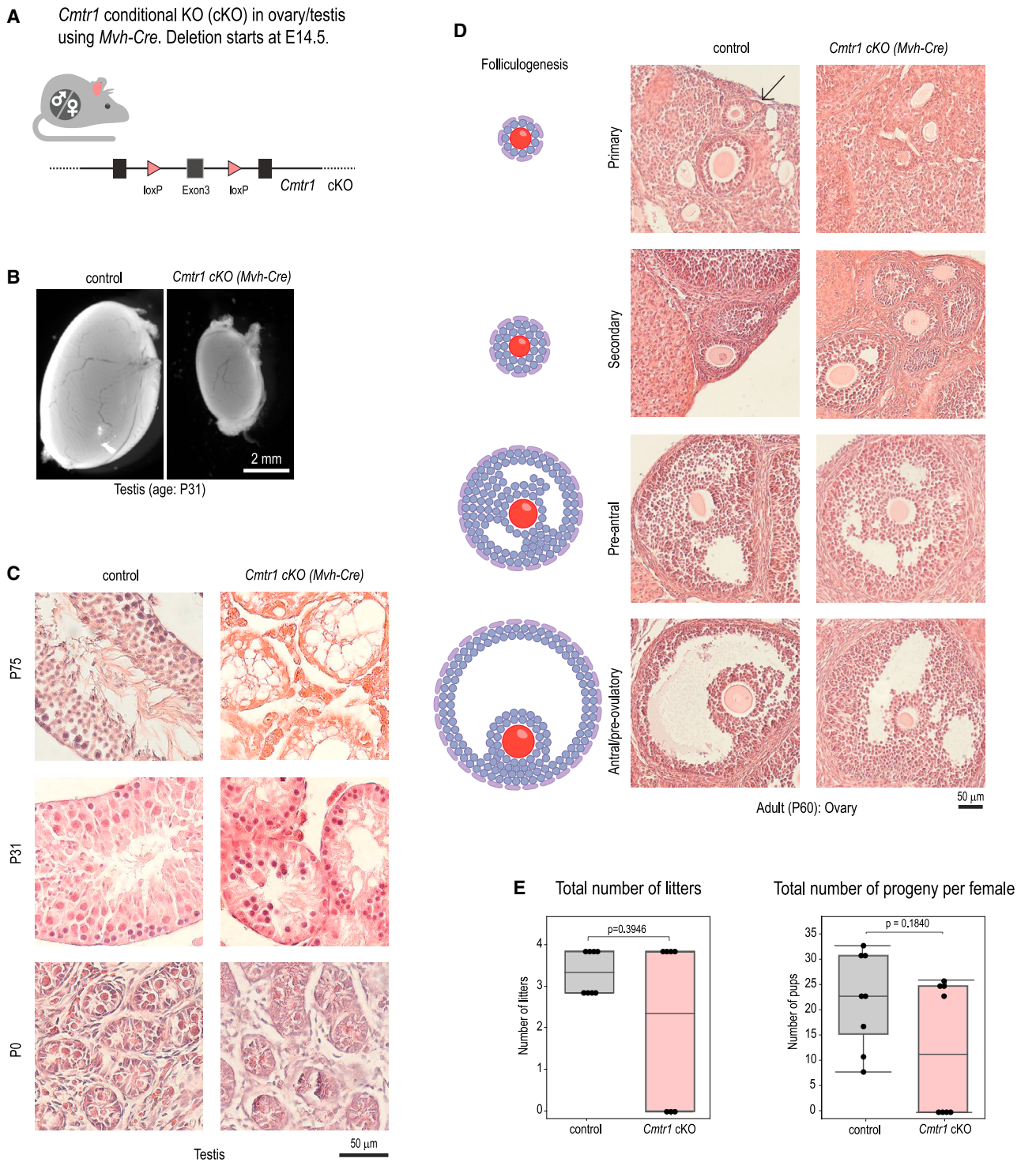

Figure 2. Mouse *Cmtr1* is essential for germline development and fertility

(A) Strategy for generating conditional knockout (cKO) deletion of *Cmtr1* in the mouse germline by deleting the coding exon3 using the *Mvh-Cre* line. See also Figure S2A.

(B) Atrophied mouse testes in the *Cmtr1* cKO ($Cmtr1^{-/loxP}$;Mvh-$Cre^{+/-}$) vs. control ($Cmtr1^{+/loxP}$;Mvh-$Cre^{+/-}$) mice. Scale bar for 2 mm is indicated.

(C) Histological analysis using hematoxylin and eosin staining of *Cmtr1* cKO and control mouse testes at different indicated postnatal stages. Scale bar for 50 μm is indicated.

(legend continued on next page)

(Figure 1G). In conclusion, the limited expression changes in E6.5 *Cmtr1* mutant embryos, including that of several snoRNA host genes, leads to large-scale changes in the E7.5 embryos causing the mid-gastrulation arrest.

Mouse CMTR1 is essential for fertility

To study the role of CMTR1 in the mouse germline, we obtained the conditional KO mice, where deletion in the germline is achieved by the germline-specific *Mvh-Cre* line (*Vasa-Cre*) (Figures 2A, S2A, and S2B and STAR Methods). Germline-specific expression of the *Mvh-Cre* starts from embryonic day E14.5, ultimately creating the *Cmtr1* conditional knockout mice (*Cmtr1*$^{loxP/-}$*; Mvh-Cre*, cKO). When *Cmtr1* cKO adult (>60 postnatal days, P60) males were crossed with wild-type females, no litters were obtained, indicating male infertility. Examination of testes from adult (P75) cKO males shows that they are highly atrophied when compared to those from control (*Cmtr1*$^{loxP/+}$*; Mvh-Cre*) littermates (Figure 2B). Histological examination shows that seminiferous tubules in the adult cKO testes are narrow and empty of all germ cells (Figure 2C). In contrast, tubules in the control testes are large and full of germ cells in all stages of development during spermatogenesis. Mitotic spermatogonia, meiotic spermatocytes, post-meiotic haploid round spermatids, elongate spermatids and sperm are all visible within the control seminiferous tubules (Figures 2C and S2C). To determine when the spermatogenic arrest manifests in the cKO males, we examined younger mice. Germ cells in the seminiferous tubules of the control and mutant neonates (P0) are comparable (Figure 2C). In P31 animals, the seminiferous tubules in the control testes are large and full of germ cells that have completed meiosis, while the tubules in the mutant testes are narrow and depleted of such germ cells (Figure 2C). We propose that germ cells in the *Cmtr1* cKO testes do not survive and are probably removed by apoptosis.

Mitotic oogonia in the embryonic female germline enter meiosis at E13.5, and the oocytes are in pachytene stage of prophase I of meiosis at birth,[44] which is immediately followed by the diplotene stage when the oocytes start to assemble a multi-cell layered follicle around them (Figure 2D). Folliculogenesis proceeds through multiple stages with primary follicles having a single layer of granulosa cells around the oocyte. Histological examination of adult ovaries from both the control and the cKO females reveals oocytes in all the different stages, including the large mature follicles (Figures 2D and S2D). When cKO females were crossed with wild-type partners, some produced litters, while others never had any progeny (Figure 2E). The overall number of pups tended to be lower with the cKO *Cmtr1* females. We note that conditional deletion of *Cmtr1* due to *Mvh*-driven Cre expression takes place only from E14.5, once meiosis is already initiated in the female germline at E13.5, explaining the low penetrance of the female infertility phenotype. Taken together, we conclude that CMTR1 is required for sustaining normal germline development and fertility in mice.

Loss of cap1 RNA methylation in mouse liver triggers the innate immune pathway

The above studies demonstrate that CMTR1 is important for developmental transitions, with its loss ultimately leading to death of the embryo or germ cells. CMTR1 is expressed in most mouse tissues (Figure 3A), and we decided to delete the *Cmtr1* in the adult mouse liver using tamoxifen-activated Cre-ERT2 that is expressed from the liver-specific albumin promoter (*Alb-CreERT2*) (Figures 3B, S3A, and S3B). Conditional knockout mice (*Cmtr1*$^{loxP/-}$*;Alb-CreERT2*, cKO) and control mice (*Cmtr1*$^{loxP/+}$*;Alb-CreERT2*) were both treated with intraperitoneal tamoxifen injections for a period of 4 days (days 1–4), and depletion of CMTR1 in the liver was monitored using western blot analysis 2 days later (Figure 3C). A complete absence of CMTR1 in the cKO mouse liver was observed (Figure 3C).

Histological analysis indicates an unchanged cellularity in the *Cmtr1* cKO liver (Figure 3D). Transcriptome analysis showed limited changes, with ~100 genes being altered in their expression (Figure 3E and Table S3). Strikingly, Gene Ontology analysis identifies an upregulation of transcripts involved in the anti-viral innate immune response pathway (Figure 3F). A number of ISGs are upregulated in the *Cmtr1* cKO liver (Figures 3E and 3G). Interferon mRNAs themselves are not detected, as they are usually expressed briefly before being turned off. We confirmed the induction of one such ISG by western blot analysis, which shows the specific expression of IFIT1 (interferon-induced protein with tetratricopeptide repeats 1) in all the *Cmtr1* cKO liver samples (Figure 3C). Analysis of the *Cmtr1* cKO mouse liver transcriptome at later time points of 6 days and 22 days post tamoxifen injection also revealed upregulation of ISG expression (Figures 3H and 3I). Thus, loss of *Cmtr1* in adult mouse liver can lead to chronic interferon pathway activation, which is accompanied by further alterations in metabolic pathway genes (Figure S3C). We note that the interferon-stimulated gene oligoadenylate synthetase like-1 (OASL1) that is induced in the mutant livers is reported as a negative regulator of interferon pathway, perhaps preventing tissue damage from chronic activation of the pathway.[45] RNA mass spectrometry analysis (STAR Methods) of polyA + RNAs from the *Cmtr1* cKO liver (sampled at day 2) confirms a sharp reduction in ribose methylation on the first nucleotide as represented by reduced levels of m^{6}Am (Figure 3J). m^{6}Am is a modification that depends on CMTR1-dependent TSS Am ribose methylation.[11,46] We propose that in the absence of CMTR1, the cellular RNA pol II ranscripts, which now have the cap0 structure, are sensed as "non-self," triggering interferon production[17] and expression of the ISGs.[47]

Loss of CMTR1 does not affect human cell viability and translation

To examine whether complete loss of CMTR1 is detrimental for cell survival, we examined a CRISPR-generated *CMTR1* knockout human HAP1 cell line (STAR Methods). HAP1 is a

(D) Histological analysis using hematoxylin and eosin staining of mouse ovaries from control and *Cmtr1* cKO is shown. The cartoon representation of the different stages of folliculogenesis is shown. Scale bar for 50 μm is indicated. Arrow points to a primary follicle.
(E) Fertility analysis of *Cmtr1* cKO females. Boxplots compare total number of litters (left) delivered and total number of progeny (right) per female. Mann-Whitney test was used to assess differences between wild-type and cKO animals. See also Figure S2D.

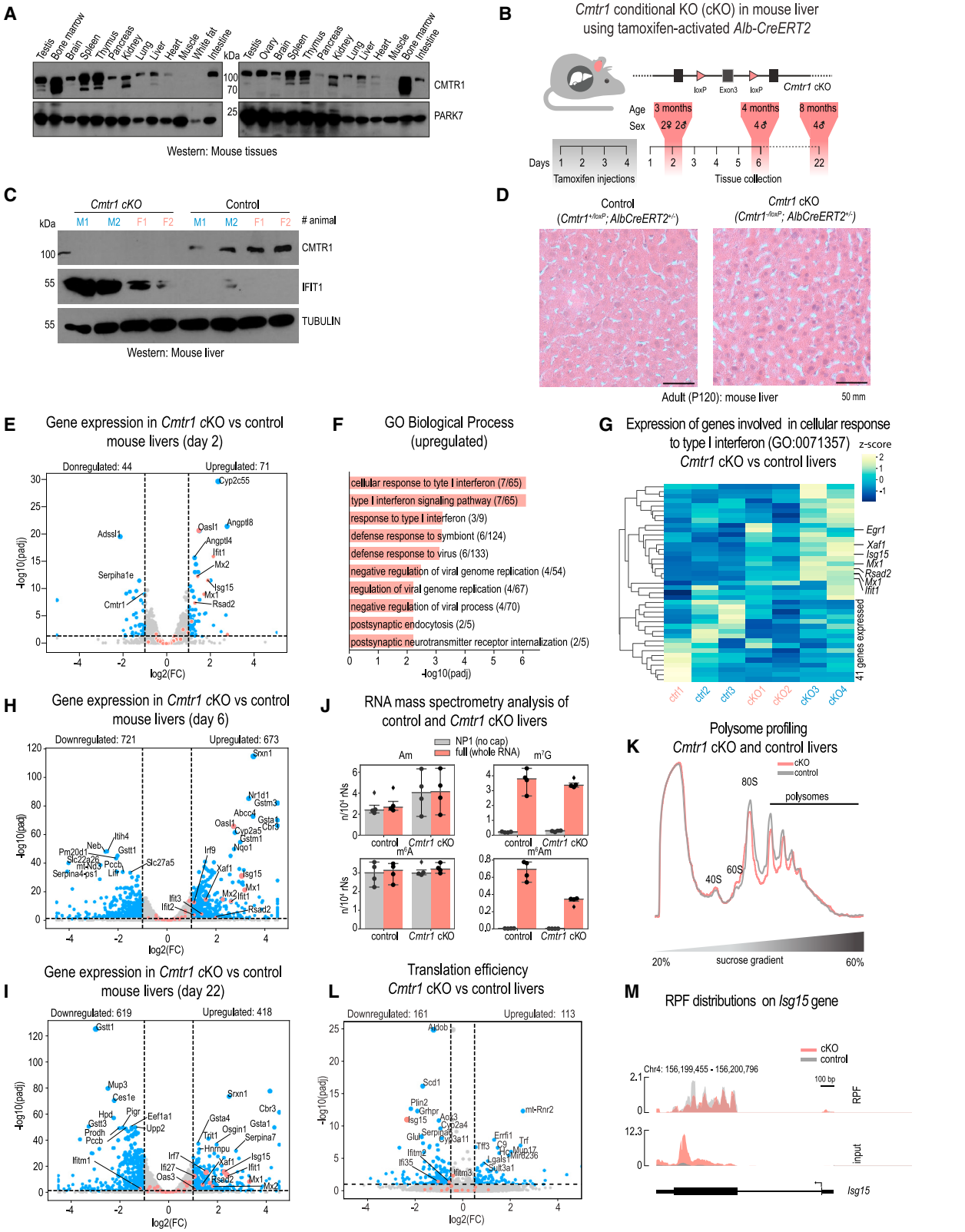

(legend on next page)

near-haploid cell line derived from the KBM-7 chronic myelogenous leukemia cell line. Complete loss of CMTR1 in these cells (Figure S4A) leads to complete loss of cap1 methylation (Figure S4B and STAR Methods). Although cell growth of the KO cell line was reduced (Figure S4C), this was not due to any impact on the cell cycle (Figure S4D). We note that reduced cell growth phenotype is observed in several unrelated mutant HAP1 cells that we have examined. We observed thousands of transcripts to be altered in the *CMTR1* KO cells but without activation of the interferon pathway (Figures S4E and S4H–S4I), probably because the innate immune sensors are not expressed in this cell line (Figure S4G).

We also examined translation status in the mutant cell line by ribosome profiling, but only a very few transcripts showed altered translation in the KO cell line (Figure S4F and Table S4). Similarly, sucrose-gradient centrifugation of *Cmtr1* cKO livers lysates did not reveal any changes in global translation as indicated by the largely identical patterns of the expected monosome and polysome peaks (Figures 3K and S3D). Ribosome profiling analysis showed that translation of only a few transcripts is altered (either increased or decreased) in the *Cmtr1* cKO liver (Figure 3L and Table S4). IFIT1 binds the cap0 structure to impair translation by competitively preventing recruitment of the translation initiation factor, cap-binding protein eIF4E.[24–26] However, we did not find any dramatic impact on translation *in vivo*. Consistent with a previous report,[48] we find that translation of *ISG15* is decreased in the absence of CMTR1 in mouse livers (Figures 3L–3M). Taken together, we show that loss of cap1 RNA methylation is not detrimental for translation of most mRNAs in the mouse liver and human HAP1 cells.

The cap2 methylase CMTR2 is essential for mouse embryonic development

Next, we obtained a mutant mouse where the entire CMTR2 coding sequence was deleted (Figures S5A and S5B and STAR Methods). Heterozygous *Cmtr2*$^{+/-}$ mice are viable and fertile. Intercrosses between heterozygous partners did not produce any homozygous *Cmtr2*$^{-/-}$ knockout (KO) mice (hereafter referred to as *Cmtr2* mutant) in the born litter, indicating pre-weaning lethality (Figures 4A and 4B). We set up crosses between heterozygous partners and genotyped embryos at different post-implantation stages (Figure S5C). This indicated that *Cmtr2* mutant embryos were present at above Mendelian ratios at E6.5 and E7.5 (Figure 4C). Mutant *Cmtr2* embryos recovered beyond E6.5 were infrequent, reduced in size, and found arrested at a preceding developmental stage (Figure S5C).

To examine the impact on gene expression in the *Cmtr2* KO, we chose E6.5 embryos that appeared morphologically similar to the control wild type. We also sequenced embryos isolated 1 day later at E7.5, where the *Cmtr2* mutant embryos are smaller than the control (Figure 4D). Sequence analysis indicates that CMTR2 regulates levels of hundreds of transcripts, most of which are upregulated in the mutant (Figure 4E and Table S3). Gene Ontology analysis revealed that genes active in many different pathways are impacted (Figures S5D–S5G). Similarly, hundreds of genes are altered in the *Cmtr2* mutant E7.5 embryos (Figure 4E). Estimation of cell composition changes from the bulk sequencing data shows that critical cell types required for normal embryonic development are affected in the *Cmtr2* mutant (Figure S5H and STAR Methods). Finally, comparison of the changes in the *Cmtr1* and *Cmtr2* mutant embryos shows that the two proteins regulate non-overlapping sets of genes (Figure 4F). In conclusion, we find that loss of the cap2 RNA methylase *Cmtr2* results in post-implantation lethality in mice, with most embryos arrested during mid-gastrulation at E7.5.

DISCUSSION

Here we showed that both *Cmtr1* and *Cmtr2* are essential for mouse embryonic development. While a role for cap1[21–23] and cap2[13,28] modifications in blocking activation of the innate immune response pathway is established, transcriptome analysis of the mutant embryos did not reveal signatures of interferon signaling. We rationalize that this is due to absence of expression of innate immune sensors at the early developmental time points (Figure 1F). Indeed, the mid-gastrulation arrest (at E7.5) of *Cmtr1*

Figure 3. Loss of *Cmtr1* in mouse liver activates the innate immune response pathway

(A) Western analysis of CMTR1 in adult (P60) mouse tissues.

(B) Strategy for generating conditional knockout (cKO) deletion of *Cmtr1* in the mouse liver using the tamoxifen activable CreERT2. Mice are given daily injections for 4 days and analyzed 2, 6, and 22 days later.

(C) Western analysis with four biological replicates of liver lysates each from control (*Cmtr1*$^{+/loxP}$; AlbCreERT2$^{+/-}$) and *Cmtr1* cKO (*Cmtr1*$^{-/loxP}$; AlbCreERT2$^{+/-}$) adult mice. TUBULIN is used as loading control. Sex of donor animal is indicated: M, male (blue); F, female (red).

(D) Histological analysis using hematoxylin and eosin staining of mouse liver from control and *Cmtr1* cKO.

(E) Volcano plot of differential gene expression in liver using transcriptome sequencing of three to four biological replicates of *Cmtr1* cKO and control adult mice. Type I IFN pathway genes are highlighted in red. Absolute log2 fold change (log2FC) cutoff = 1; adjusted p value (padj) cutoff = 0.05.

(F) Gene ontology analysis of the genes upregulated in the *Cmtr1* cKO adult mouse liver compared to the control.

(G) Heatmap showing expression changes of the 41 genes involved in cellular response to the type I interferon (GO:0071357) in the control and *Cmtr1* cKO mouse liver. Data for the three to four biological replicates are shown. Males (blue) and females (red) are shown in different colors.

(H and I) Volcano plot of differential gene expression between *Cmtr1* cKO and control adult mice from day 6 or day 22 post injection. Type I IFN pathway genes are highlighted in red. Absolute log2 fold change (log2FC) cutoff = 1; adjusted p value (padj) cutoff = 0.05. See also Figure S3C.

(J) PolyA+ RNA from *Cmtr1* control and cKO livers was subjected to mass spectrometry. Bar plots combined with boxplots show abundance (number of modified nucleotides/10^4 nucleotides) of some of the modifications (Am, m^7G, m^6A, m^6Am). Quadruplicate biological replicates were tested.

(K) Sucrose density gradient (linear 20%–60%) analysis of liver lysates from control and the *Cmtr1* cKO adult mouse. Positions of 40S and 60S subunits, 80S monosomes, and the polysome peaks are indicated. See also Figure S3D for second replicate.

(L) The volcano plot of differential translation efficiency of liver transcripts between *Cmtr1* cKO and control mice. *Isg15* is highlighted in red. Absolute log2 fold change (log2FC) cutoff = 0.5, and adjusted p value (padj) cutoff = 0.05.

(M) Normalized coverage tracks of *Isg15* counts (rpm) from the merged ribosome-protected fragment (RPF) and input samples. See also Figure S3E.

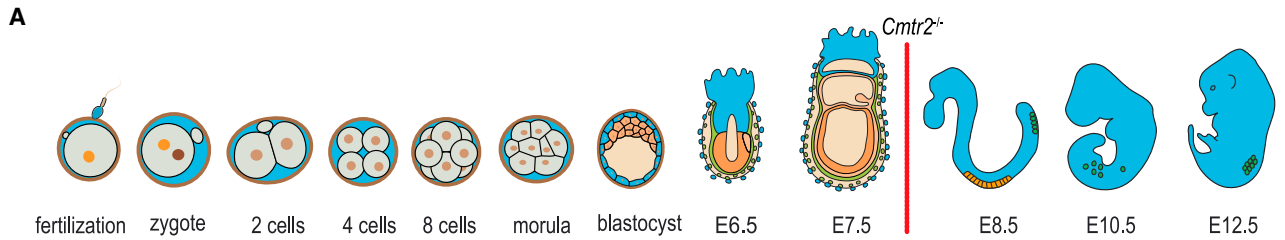

B

Cmtr2 HET x HET

TOTAL	WT	HET	KO
56	21	35	0
	37.5%	62.5%	0%

C

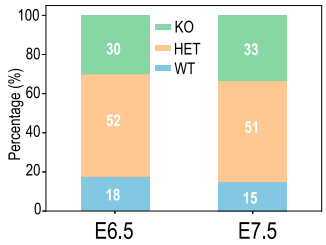

D

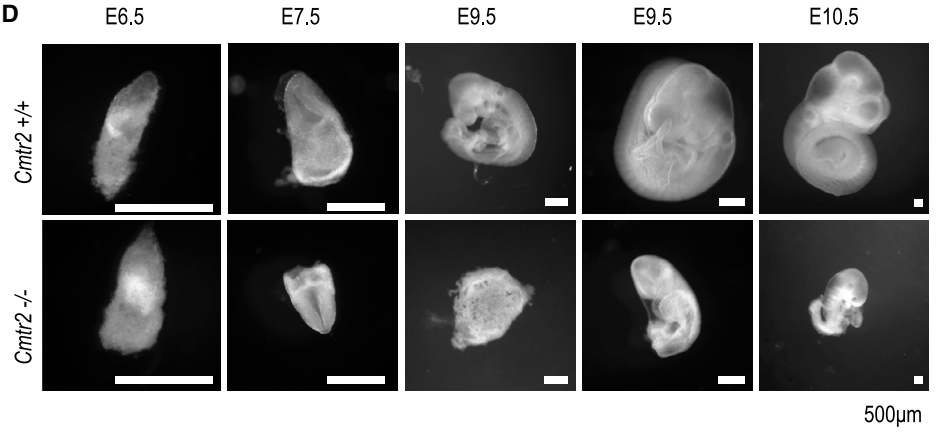

E

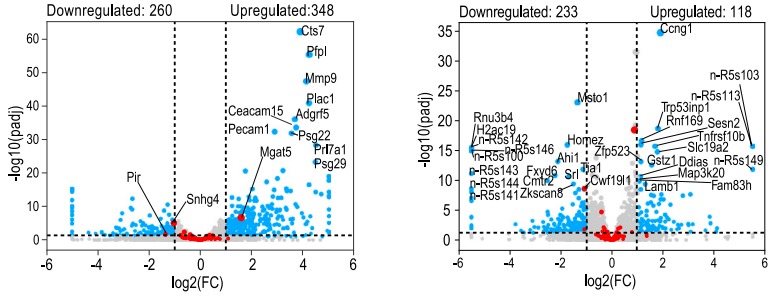

F

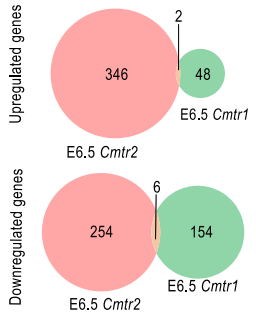

Figure 4. *Cmtr2* is essential for mouse embryonic development

(A) Scheme of embryonic development with lethality in *Cmtr2* mutants indicated by a red line.

(B) Genotypes of animals (at weaning age) born out of heterozygous *Cmtr2* mouse crosses. WT, wild type; HET, heterozygous; KO, homozygous knockout. See also Figure S5C.

(C) Genotypes of mouse embryos (shown as percentage) at indicated embryonic days.

(D) Pictures of representative wild-type and *Cmtr2* KO embryos at different stages are shown. The mutant embryos start to disintegrate already from E7.5 onward.

(E) Volcano plots showing differentially expressed genes between *Cmtr2* KO and wild-type E6.5 and E7.5 mouse embryos. snoRNA host genes are highlighted in red. Absolute log2 fold change (log2FC) cutoff = 1; adjusted p value (padj) cutoff = 0.05.

(F) Venn diagrams showing lack of overlap in gene expression changes in the *Cmtr1* and *Cmtr2* KO mouse embryos compared to their wild-type controls.

and *Cmtr2* mutant mouse embryos contrasts with the late arrest seen in the mutant embryos for *Adar1* (adenosine deaminase acting on RNA).[49,50] *Adar1* mutant embryos die due to activation of the interferon pathway in an MDA5-dependent manner only at E12.5 to E13.5, a time window when the innate immune receptors start to be expressed (Figures 1F and S1D). This suggests that cap1 and cap2 modifications have an essential role in shaping gene expression early during mammalian embryonic development that is unrelated to their role in marking host RNAs as "self."

Transcriptome analysis shows that the two proteins regulate non-overlapping sets of genes (Figure 4F). This points to distinct RNA targets, which is consistent with the distinct sub-cellular compartments where the two enzymes act.

CMTR1 can co-transcriptionally engage the nascent RNA via interaction of its WW domain with the CTD of RNA pol II.[29,30] Methylation by CMTR2 on the other hand is reported to be cytosolic.[51] How ribose methylations affect target gene expression is not clear. Perhaps proteins that bind the cap structure and sense the proximal nucleotides are influenced by the methylations. However, binding affinity of the recombinant human nuclear Cap-binding complex (CBC) for the m^7G cap analog (m^7GpppN vs. $m^7GpppNm$) is not influenced by the cap1 modification.[52] Likewise, affinity of the recombinant mouse translation initiation factor eIF4E for the cap structure is not affected by presence of the cap1 or cap2.[28] Nevertheless, analysis using fly nuclear extracts shows an increased association between the fly CBC component CBC80 and cap2 RNA, when compared to the cap0 RNA control.[32] It is also known that cap-proximal ribose methylations can influence cap-binding of factors involved in the innate immune response pathway.[21,24–26] Furthermore, protein factors that interact with the cap methylases may modulate their activity or targeting. CMTR1 is shown to interact with the RNA helicase DHX15 (Figure S4J), with the interaction reducing RNA methylation activity of CMTR1[53] or promoting its activity on RNAs with secondary structures.[54]

In the case of *Cmtr1* mutant embryos, we reported downregulation of several snoRNA host genes. We speculate that presence of cap1 modification might facilitate coordinated processing of the intron-resident snoRNAs and splicing of the intron. It also remains an exciting possibility that the unavailability of specific snoRNAs might underlie embryonic arrest phenotype in the *Cmtr1* mutant. However, this impact on snoRNA host genes was not seen in the *Cmtr1* mutant liver (Figure S3G) and human *CMTR1* KO HAP1 cells (Figure S4F). While we refer to genes being regulated as those that are increased or decreased in levels in the mutant environment, we are unable to precisely determine the molecular reason for these changes. There are different possibilities, as CMTR1 is proposed to promote transcription,[30] RNA splicing,[55] stability,[9] or association with cap-binding factors to promote RNA localization.[32] Our examination of translation in the *Cmtr1* mutant liver (Figures 3K and S3F) and human knockout cell line (Figure S4F) shows that global translation is unaffected.

Our *Cmtr2* mutant embryo analysis shows that the misregulated genes are distinct from those affected in the *Cmtr1* mutant (Figure 4F). Precise mapping of cap2 on transcripts expressed in human HEK293T cells shows that transcripts tend to accumulate the modification without any particular sequence.[13] The level of cap2 is also variable in different tissue and cell types. The same study concluded that translation and RNA stability were not influenced by the presence of the cap2 modification,[13] while another study showed that presence of cap2 reduces translation of reporter mRNAs in some cell types.[28] Cap2-modified RNA was shown to resist recognition by the innate immune sensor RIG-I, thereby preventing activation of the interferon signaling pathway[13] or by reducing binding of the interferon-stimulated gene IFIT1, which acts as a translation repressor.[24] In conclusion, our study sheds light on a role for cap1 and cap2 methylation in gene regulation, beyond their role in marking cellular RNAs as "self."

Limitations of the study

While we described the transcriptome changes in the mutant embryos, we are unable to say if these are direct effects due to loss of the respective proteins and due to loss of position-specific ribose methylations on these RNAs. While we documented reduced transcript levels of some of the snoRNA host genes in the *Cmtr1* mutant embryos, we could not evaluate if this affected the levels of the intron-encoded snoRNAs. We showed that CMTR1 is essential for germline development as mutant males are completely infertile, while females display infertility at low penetrance. However, we do not know if this is due to a direct role in germline gene expression or due to activation of the interferon pathway, as observed in the conditional *Cmtr1* mutant livers (Figure 2E). Finally, the molecular role of cap2 methylation in gene regulation and how CMTR2 selects its target RNAs remain open questions.

STAR★METHODS

Detailed methods are provided in the online version of this paper and include the following:

- KEY RESOURCES TABLE
- RESOURCE AVAILABILITY
  - Lead contact
  - Materials availability
  - Data and code availability
- EXPERIMENTAL MODEL AND STUDY PARTICIPANT DETAILS
  - Animal work
  - Mouse mutants
  - Human HAP1 *CMTR1* KO cells
- METHOD DETAILS
  - *Cmtr1* knockout mouse
  - *Cmtr2* knockout mouse
  - Creation of *Cmtr1 loxP* mice
  - Tamoxifen-inducible conditional *Cmtr1* deletion in mouse liver
  - Conditional *Cmtr1* germline knockout mice
  - Mouse genotyping
  - Collection of mouse embryos
  - Human HAP1 *CMTR1* KO cells
  - Clones and constructs
  - Recombinant protein production
  - Purification of mouse CMTR2 protein
  - Purification of human CMTR1-DHX15 complex
  - Antibodies
  - Collection of RNA from HAP1 cells
  - RNA extraction from cell lines
  - Growth curve
  - Analysis of cell cycle by FACS
  - Collecting mouse tissues for western blot
  - Western Blot
  - Histological analysis of mouse tissues
  - Total RNA purification from mouse liver samples
  - PolyA+ RNA purification
  - Quantification of RNA modifications using LC-MS/MS
  - RNA library preparation and sequencing

SUPPLEMENTAL INFORMATION

Supplemental information can be found online at https://doi.org/10.1016/j.celrep.2023.112786.

ACKNOWLEDGMENTS

We thank Nicolas Roggli for scientific illustration and Pascal Gos for help with mouse work. We thank the Mouse Knockout Program and the Mutant Mouse Resource and Research Center (MMRRC), University of California at Davis for mouse mutants. We thank the following University of Geneva core facilities: iGE3 Genomics Platform, Transgenic Mouse Facility, Histology Facility. We also thank the EMBL Genomics core facility for deep sequencing. We thank fellowships to the students: M.D. (Swiss Government Excellence PhD Scholarship), K.K. (NCCR RNA&Disease network), M.M. (Boehringer Ingelheim Fonds PhD Fellowship), and L.L. (iGE3 PhD Fellowship). This work was supported by grants to R.S.P. from the Swiss National Science Foundation: Project Grant (#310030_207468), Sinergia Grant (#CRSII5_186266) and funding from the NCCR RNA & Disease (#51NF40-205601). Work in the Pillai lab is supported by the Republic and Canton of Geneva.

AUTHOR CONTRIBUTIONS

M.D. conducted a majority of the experiments including all the mouse experiments and cell culture work; K.K. did all computational analyses and prepared all the figures with M.D.; M.M. prepared the conditional *Cmtr1* KO mouse; L.L. produced recombinant proteins; O.P. did ribosome and polysome profiling; F.F.-O. prepared RNAs from mouse tissues; C.B.V. did RNA mass spectrometry analyses; D.H. helped with computational analyses at an early stage of this study; manuscript preparation was by R.S.P. with input from everyone.

DECLARATION OF INTERESTS

The authors declare no competing interests.

Received: February 1, 2023
Revised: May 11, 2023
Accepted: June 25, 2023
Published: July 11, 2023

REFERENCES

1. Wei, C.M., Gershowitz, A., and Moss, B. (1975). Methylated nucleotides block 5' terminus of HeLa cell messenger RNA. Cell *4*, 379–386. https://doi.org/10.1016/0092-8674(75)90158-0.
2. Furuichi, Y., Morgan, M., Muthukrishnan, S., and Shatkin, A.J. (1975). Reovirus messenger RNA contains a methylated, blocked 5'-terminal structure: m-7G(5')ppp(5')G-MpCp. Proc. Natl. Acad. Sci. USA *72*, 362–366. https://doi.org/10.1073/pnas.72.1.362.
3. Furuichi, Y., Muthukrishnan, S., and Shatkin, A.J. (1975). 5'-Terminal m-7G(5')ppp(5')G-m-p in vivo: identification in reovirus genome RNA. Proc. Natl. Acad. Sci. USA *72*, 742–745. https://doi.org/10.1073/pnas.72.2.742.
4. Furuichi, Y., Morgan, M., Shatkin, A.J., Jelinek, W., Salditt-Georgieff, M., and Darnell, J.E. (1975). Methylated, blocked 5 termini in HeLa cell mRNA. Proc. Natl. Acad. Sci. USA *72*, 1904–1908.
5. Wei, C.M., and Moss, B. (1975). Methylated nucleotides block 5'-terminus of vaccinia virus messenger RNA. Proc. Natl. Acad. Sci. USA *72*, 318–322.
6. Perry, R.P., and Kelley, D.E. (1975). Methylated constituents of heterogeneous nuclear RNA: presence in blocked 5' terminal structures. Cell *6*, 13–19. https://doi.org/10.1016/0092-8674(75)90068-9.
7. Furuichi, Y., and Shatkin, A.J. (2000). Viral and cellular mRNA capping: past and prospects. Adv. Virus Res. *55*, 135–184.
8. Muthukrishnan, S., Filipowicz, W., Sierra, J.M., Both, G.W., Shatkin, A.J., and Ochoa, S. (1975). mRNA methylation and protein synthesis in extracts from embryos of brine shrimp, Artemia salina. J. Biol. Chem. *250*, 9336–9341.
9. Picard-Jean, F., Brand, C., Tremblay-Létourneau, M., Allaire, A., Beaudoin, M.C., Boudreault, S., Duval, C., Rainville-Sirois, J., Robert, F., Pelletier, J., et al. (2018). 2'-O-methylation of the mRNA cap protects RNAs from decapping and degradation by DXO. PLoS One *13*, e0193804. https://doi.org/10.1371/journal.pone.0193804.
10. Bélanger, F., Stepinski, J., Darzynkiewicz, E., and Pelletier, J. (2010). Characterization of hMTr1, a human Cap1 2'-O-ribose methyltransferase. J. Biol. Chem. *285*, 33037–33044. https://doi.org/10.1074/jbc.M110.155283.
11. Akichika, S., Hirano, S., Shichino, Y., Suzuki, T., Nishimasu, H., Ishitani, R., Sugita, A., Hirose, Y., Iwasaki, S., Nureki, O., and Suzuki, T. (2019). Cap-specific terminal N (6)-methylation of RNA by an RNA polymerase II-associated methyltransferase. Science *363*, eaav0080. https://doi.org/10.1126/science.aav0080.
12. Werner, M., Purta, E., Kaminska, K.H., Cymerman, I.A., Campbell, D.A., Mittra, B., Zamudio, J.R., Sturm, N.R., Jaworski, J., and Bujnicki, J.M. (2011). 2'-O-ribose methylation of cap2 in human: function and evolution in a horizontally mobile family. Nucleic Acids Res. *39*, 4756–4768. https://doi.org/10.1093/nar/gkr038.
13. Despic, V., and Jaffrey, S.R. (2023). mRNA ageing shapes the Cap2 methylome in mammalian mRNA. Nature *614*, 358–366.
14. Habjan, M., and Pichlmair, A. (2015). Cytoplasmic sensing of viral nucleic acids. Curr. Opin. Virol. *11*, 31–37.
15. Kowalinski, E., Lunardi, T., McCarthy, A.A., Louber, J., Brunel, J., Grigorov, B., Gerlier, D., and Cusack, S. (2011). Structural basis for the activation of innate immune pattern-recognition receptor RIG-I by viral RNA. Cell *147*, 423–435.
16. Luo, D., Ding, S.C., Vela, A., Kohlway, A., Lindenbach, B.D., and Pyle, A.M. (2011). Structural insights into RNA recognition by RIG-I. Cell *147*, 409–422.
17. Ivashkiv, L.B., and Donlin, L.T. (2014). Regulation of type I interferon responses. Nat. Rev. Immunol. *14*, 36–49.
18. Schoggins, J.W., Wilson, S.J., Panis, M., Murphy, M.Y., Jones, C.T., Bieniasz, P., and Rice, C.M. (2011). A diverse range of gene products are effectors of the type I interferon antiviral response. Nature *472*, 481–485.
19. Daffis, S., Szretter, K.J., Schriewer, J., Li, J., Youn, S., Errett, J., Lin, T.Y., Schneller, S., Zust, R., Dong, H., et al. (2010). 2'-O methylation of the viral mRNA cap evades host restriction by IFIT family members. Nature *468*, 452–456. https://doi.org/10.1038/nature09489.
20. Züst, R., Cervantes-Barragan, L., Habjan, M., Maier, R., Neuman, B.W., Ziebuhr, J., Szretter, K.J., Baker, S.C., Barchet, W., Diamond, M.S., et al. (2011). Ribose 2'-O-methylation provides a molecular signature for the distinction of self and non-self mRNA dependent on the RNA sensor Mda5. Nat. Immunol. *12*, 137–143. https://doi.org/10.1038/ni.1979.
21. Schuberth-Wagner, C., Ludwig, J., Bruder, A.K., Herzner, A.M., Zillinger, T., Goldeck, M., Schmidt, T., Schmid-Burgk, J.L., Kerber, R., Wolter, S.,

et al. (2015). A Conserved Histidine in the RNA Sensor RIG-I Controls Immune Tolerance to N1-2'O-Methylated Self RNA. Immunity *43*, 41–51. https://doi.org/10.1016/j.immuni.2015.06.015.

22. Wang, Y., Ludwig, J., Schuberth, C., Goldeck, M., Schlee, M., Li, H., Juranek, S., Sheng, G., Micura, R., Tuschl, T., et al. (2010). Structural and functional insights into 5′-ppp RNA pattern recognition by the innate immune receptor RIG-I. Nat. Struct. Mol. Biol. *17*, 781–787.

23. Devarkar, S.C., Wang, C., Miller, M.T., Ramanathan, A., Jiang, F., Khan, A.G., Patel, S.S., and Marcotrigiano, J. (2016). Structural basis for m7G recognition and 2′-O-methyl discrimination in capped RNAs by the innate immune receptor RIG-I. Proc. Natl. Acad. Sci. USA *113*, 596–601.

24. Abbas, Y.M., Laudenbach, B.T., Martínez-Montero, S., Cencic, R., Habjan, M., Pichlmair, A., Damha, M.J., Pelletier, J., and Nagar, B. (2017). Structure of human IFIT1 with capped RNA reveals adaptable mRNA binding and mechanisms for sensing N1 and N2 ribose 2'-O methylations. Proc. Natl. Acad. Sci. USA *114*, E2106–E2115. https://doi.org/10.1073/pnas.1612444114.

25. Habjan, M., Hubel, P., Lacerda, L., Benda, C., Holze, C., Eberl, C.H., Mann, A., Kindler, E., Gil-Cruz, C., Ziebuhr, J., et al. (2013). Sequestration by IFIT1 impairs translation of 2′ O-unmethylated capped RNA. PLoS Pathog. *9*, e1003663.

26. Fleith, R.C., Mears, H.V., Leong, X.Y., Sanford, T.J., Emmott, E., Graham, S.C., Mansur, D.S., and Sweeney, T.R. (2018). IFIT3 and IFIT2/3 promote IFIT1-mediated translation inhibition by enhancing binding to non-self RNA. Nucleic Acids Res. *46*, 5269–5285.

27. Li, B., Clohisey, S.M., Chia, B.S., Wang, B., Cui, A., Eisenhaure, T., Schweitzer, L.D., Hoover, P., Parkinson, N.J., Nachshon, A., et al. (2020). Genome-wide CRISPR screen identifies host dependency factors for influenza A virus infection. Nat. Commun. *11*, 164. https://doi.org/10.1038/s41467-019-13965-x.

28. Drazkowska, K., Tomecki, R., Warminski, M., Baran, N., Cysewski, D., Depaix, A., Kasprzyk, R., Kowalska, J., Jemielity, J., and Sikorski, P.J. (2022). 2′-O-Methylation of the second transcribed nucleotide within the mRNA 5′ cap impacts the protein production level in a cell-specific manner and contributes to RNA immune evasion. Nucleic Acids Res. *50*, 9051–9071.

29. Haline-Vaz, T., Silva, T.C.L., and Zanchin, N.I.T. (2008). The human interferon-regulated ISG95 protein interacts with RNA polymerase II and shows methyltransferase activity. Biochem. Biophys. Res. Commun. *372*, 719–724. https://doi.org/10.1016/j.bbrc.2008.05.137.

30. Liang, S., Silva, J.C., Suska, O., Lukoszek, R., Almohammed, R., and Cowling, V.H. (2022). CMTR1 is recruited to transcription start sites and promotes ribosomal protein and histone gene expression in embryonic stem cells. Nucleic Acids Res. *50*, 2905–2922. https://doi.org/10.1093/nar/gkac122.

31. Lee, Y.-L., Kung, F.-C., Lin, C.-H., and Huang, Y.-S. (2020). CMTR1-Catalyzed 2′-O-Ribose Methylation Controls Neuronal Development by Regulating Camk2α Expression Independent of RIG-I Signaling. Cell Rep. *33*, 108269.

32. Haussmann, I.U., Wu, Y., Nallasivan, M.P., Archer, N., Bodi, Z., Hebenstreit, D., Waddell, S., Fray, R., and Soller, M. (2022). CMTr cap-adjacent 2′-O-ribose mRNA methyltransferases are required for reward learning and mRNA localization to synapses. Nat. Commun. *13*, 1209–1213.

33. Tam, P.P.L., and Loebel, D.A.F. (2007). Gene function in mouse embryogenesis: get set for gastrulation. Nat. Rev. Genet. *8*, 368–381.

34. O'Brien, S.J., Fiechter, C., Burton, J., Hallion, J., Paas, M., Patel, A., Patel, A., Rochet, A., Scheurlen, K., Gardner, S., et al. (2021). Long noncoding RNA ZFAS1 is a major regulator of epithelial-mesenchymal transition through miR-200/ZEB1/E-cadherin, vimentin signaling in colon adenocarcinoma. Cell Death Discov. *7*, 61. https://doi.org/10.1038/s41420-021-00427-x.

35. Kiss, T. (2004). Biogenesis of small nuclear RNPs. J. Cell Sci. *117*, 5949–5951.

36. Decatur, W.A., and Fournier, M.J. (2002). rRNA modifications and ribosome function. Trends Biochem. Sci. *27*, 344–351. https://doi.org/10.1016/s0968-0004(02)02109-6.

37. Terns, M.P., and Terns, R.M. (2002). Small nucleolar RNAs: versatile trans-acting molecules of ancient evolutionary origin. Gene Expr. *10*, 17–39.

38. Tycowski, K.T., Shu, M.D., Kukoyi, A., and Steitz, J.A. (2009). A conserved WD40 protein binds the Cajal body localization signal of scaRNP particles. Mol. Cell *34*, 47–57. https://doi.org/10.1016/j.molcel.2009.02.020.

39. Hirose, T., and Steitz, J.A. (2001). Position within the host intron is critical for efficient processing of box C/D snoRNAs in mammalian cells. Proc. Natl. Acad. Sci. USA *98*, 12914–12919.

40. Hirose, T., Shu, M.-D., and Steitz, J.A. (2003). Splicing-dependent and-independent modes of assembly for intron-encoded box C/D snoRNPs in mammalian cells. Mol. Cell *12*, 113–123.

41. Edery, I., and Sonenberg, N. (1985). Cap-dependent RNA splicing in a HeLa nuclear extract. Proc. Natl. Acad. Sci. USA *82*, 7590–7594.

42. Izaurralde, E., Lewis, J., McGuigan, C., Jankowska, M., Darzynkiewicz, E., and Mattaj, I.W. (1994). A nuclear cap binding protein complex involved in pre-mRNA splicing. Cell *78*, 657–668.

43. Konarska, M.M., Padgett, R.A., and Sharp, P.A. (1984). Recognition of cap structure in splicing in vitro of mRNA precursors. Cell *38*, 731–736.

44. Li, R., and Albertini, D.F. (2013). The road to maturation: somatic cell interaction and self-organization of the mammalian oocyte. Nat. Rev. Mol. Cell Biol. *14*, 141–152.

45. Lee, M.S., Kim, B., Oh, G.T., and Kim, Y.-J. (2013). OASL1 inhibits translation of the type I interferon–regulating transcription factor IRF7. Nat. Immunol. *14*, 346–355.

46. Boulias, K., Toczydłowska-Socha, D., Hawley, B.R., Liberman, N., Takashima, K., Zaccara, S., Guez, T., Vasseur, J.J., Debart, F., Aravind, L., et al. (2019). Identification of the m(6)Am Methyltransferase PCIF1 Reveals the Location and Functions of m(6)Am in the Transcriptome. Mol. Cell *75*, 631–643.e8. https://doi.org/10.1016/j.molcel.2019.06.006.

47. Schneider, W.M., Chevillotte, M.D., and Rice, C.M. (2014). Interferon-stimulated genes: a complex web of host defenses. Annu. Rev. Immunol. *32*, 513–545.

48. Williams, G.D., Gokhale, N.S., Snider, D.L., and Horner, S.M. (2020). The mRNA Cap 2′-O-Methyltransferase CMTR1 Regulates the Expression of Certain Interferon-Stimulated Genes. mSphere *5*, e00202-20–e00220.

49. Liddicoat, B.J., Piskol, R., Chalk, A.M., Ramaswami, G., Higuchi, M., Hartner, J.C., Li, J.B., Seeburg, P.H., and Walkley, C.R. (2015). RNA editing by ADAR1 prevents MDA5 sensing of endogenous dsRNA as nonself. Science *349*, 1115–1120.

50. Mannion, N.M., Greenwood, S.M., Young, R., Cox, S., Brindle, J., Read, D., Nellåker, C., Vesely, C., Ponting, C.P., McLaughlin, P.J., et al. (2014). The RNA-editing enzyme ADAR1 controls innate immune responses to RNA. Cell Rep. *9*, 1482–1494.

51. Langberg, S.R., and Moss, B. (1981). Post-transcriptional modifications of mRNA. Purification and characterization of cap I and cap II RNA (nucleoside-2'-)-methyltransferases from HeLa cells. J. Biol. Chem. *256*, 10054–10060.

52. Worch, R., Niedzwiecka, A., Stepinski, J., Mazza, C., Jankowska-Anyszka, M., Darzynkiewicz, E., Cusack, S., and Stolarski, R. (2005). Specificity of recognition of mRNA 5′ cap by human nuclear cap-binding complex. Rna *11*, 1355–1363.

53. Inesta-Vaquera, F., Chaugule, V.K., Galloway, A., Chandler, L., Rojas-Fernandez, A., Weidlich, S., Peggie, M., and Cowling, V.H. (2018). DHX15 regulates CMTR1-dependent gene expression and cell proliferation. Life Sci. Alliance *1*, e201800092. https://doi.org/10.26508/lsa.201800092.

54. Toczydlowska-Socha, D., Zielinska, M.M., Kurkowska, M., Astha, Almeida, C.F., Almeida, C.F., Stefaniak, F., Purta, E., and Bujnicki, J.M. (2018). Human RNA cap1 methyltransferase CMTr1 cooperates with RNA helicase DHX15 to modify RNAs with highly structured 5′ termini. Philos. Trans. R. Soc. Lond. B Biol. Sci. *373*, 20180161.

55. Dönmez, G., Hartmuth, K., and Lührmann, R. (2004). Modified nucleotides at the 5' end of human U2 snRNA are required for spliceosomal E-complex formation. RNA *10*, 1925–1933. https://doi.org/10.1261/rna.7186504.

56. Schuler, M., Dierich, A., Chambon, P., and Metzger, D. (2004). Efficient temporally controlled targeted somatic mutagenesis in hepatocytes of the mouse. Genesis *39*, 167–172.

57. Chen, E.Y., Tan, C.M., Kou, Y., Duan, Q., Wang, Z., Meirelles, G.V., Clark, N.R., and Ma'ayan, A. (2013). Enrichr: interactive and collaborative HTML5 gene list enrichment analysis tool. BMC Bioinf. *14*, 128. https://doi.org/10.1186/1471-2105-14-128.

58. Kuleshov, M.V., Jones, M.R., Rouillard, A.D., Fernandez, N.F., Duan, Q., Wang, Z., Koplev, S., Jenkins, S.L., Jagodnik, K.M., Lachmann, A., et al. (2016). Enrichr: a comprehensive gene set enrichment analysis web server 2016 update. Nucleic Acids Res. *44*, W90–W97. https://doi.org/10.1093/nar/gkw377.

59. R Core Team (2017). R: A Language and Environment for Statistical Computing (R Foundation for Statistical Computing).

60. Love, M.I., Huber, W., and Anders, S. (2014). Moderated estimation of fold change and dispersion for RNA-seq data with DESeq2. Genome Biol. *15*, 550. https://doi.org/10.1186/s13059-014-0550-8.

61. Huber, W., Carey, V.J., Gentleman, R., Anders, S., Carlson, M., Carvalho, B.S., Bravo, H.C., Davis, S., Gatto, L., Girke, T., et al. (2015). Orchestrating high-throughput genomic analysis with Bioconductor. Nat. Methods *12*, 115–121. https://doi.org/10.1038/nmeth.3252.

62. Patro, R., Duggal, G., Love, M.I., Irizarry, R.A., and Kingsford, C. (2017). Salmon provides fast and bias-aware quantification of transcript expression. Nat. Methods *14*, 417–419. https://doi.org/10.1038/nmeth.4197.

63. Andrews, S. (2012). FastQC: A Quality Control Application for High Throughput Sequence Data. Babraham Institute Project page. http://www. bioinformatics. bbsrc. ac. uk/projects/fastqc.

64. Dodt, M., Roehr, J.T., Ahmed, R., and Dieterich, C. (2012). FLEXBAR—flexible barcode and adapter processing for next-generation sequencing platforms. Biology *1*, 895–905.

65. Dobin, A., Davis, C.A., Schlesinger, F., Drenkow, J., Zaleski, C., Jha, S., Batut, P., Chaisson, M., and Gingeras, T.R. (2013). STAR: ultrafast universal RNA-seq aligner. Bioinformatics *29*, 15–21.

66. Waskom, M. (2021). Seaborn: statistical data visualization. J. Open Source Softw. *6*, 3021.

67. Hunter, J.D. (2007). Matplotlib: A 2D graphics environment. Comput. Sci. Eng. *9*, 90–95.

68. Fang, Z., Liu, X., and Peltz, G. (2023). GSEApy: a comprehensive package for performing gene set enrichment analysis in Python. Bioinformatics *39*, btac757.

69. Langmead, B., Trapnell, C., Pop, M., and Salzberg, S.L. (2009). Ultrafast and memory-efficient alignment of short DNA sequences to the human genome. Genome Biol. *10*, R25. https://doi.org/10.1186/gb-2009-10-3-r25.

70. Toolkit, P. (2019). Broad institute, GitHub repository.

71. Xiao, Z., Huang, R., Xing, X., Chen, Y., Deng, H., and Yang, X. (2018). De novo annotation and characterization of the translatome with ribosome profiling data. Nucleic Acids Res. *46*, e61.

72. Kurtenbach, S., and Harbour, J.W. (2019). SparK: A Publication-Quality NGS Visualization Tool. bioRxiv845529, . Preprint at. https://doi.org/10.1101/845529.

73. Trincado, J.L., Entizne, J.C., Hysenaj, G., Singh, B., Skalic, M., Elliott, D.J., and Eyras, E. (2018). SUPPA2: fast, accurate, and uncertainty-aware differential splicing analysis across multiple conditions. Genome Biol. *19*. 40-11.

74. Dong, M., Thennavan, A., Urrutia, E., Li, Y., Perou, C.M., Zou, F., and Jiang, Y. (2021). SCDC: bulk gene expression deconvolution by multiple single-cell RNA sequencing references. Brief. Bioinform. *22*, 416–427.

75. Leek, J.T., Johnson, W.E., Parker, H.S., Fertig, E.J., Jaffe, A.E., Storey, J.D., Zhang, Y., and Torres, L.C. (2014). The sva package for removing batch effects and other unwanted variation in high-throughput experiments. Bioinformatics *28*, 882–883. https://doi.org/10.1093/bioinformatics/bts034.

76. Dunn, J.G., and Weissman, J.S. (2016). Plastid: nucleotide-resolution analysis of next-generation sequencing and genomics data. BMC Genom. *17*, 958–1012.

77. Pedregosa, F., Varoquaux, G., Gramfort, A., Michel, V., Thirion, B., Grisel, O., Blondel, M., Prettenhofer, P., Weiss, R., and Dubourg, V. (2011). Scikit-learn: Machine learning in Python. J. Mach. Learn. Res. *12*, 2825–2830.

78. Gallardo, T., Shirley, L., John, G.B., and Castrillon, D.H. (2007). Generation of a germ cell-specific mouse transgenic Cre line. Genesis *45*, 413–417.

79. Ingolia, N.T., Ghaemmaghami, S., Newman, J.R.S., and Weissman, J.S. (2009). Genome-wide analysis in vivo of translation with nucleotide resolution using ribosome profiling. Science *324*, 218–223. https://doi.org/10.1126/science.1168978.

80. McGlincy, N.J., and Ingolia, N.T. (2017). Transcriptome-wide measurement of translation by ribosome profiling. Methods *126*, 112–129. https://doi.org/10.1016/j.ymeth.2017.05.028.

81. Ernst, C., Eling, N., Martinez-Jimenez, C.P., Marioni, J.C., and Odom, D.T. (2019). Staged developmental mapping and X chromosome transcriptional dynamics during mouse spermatogenesis. Nat. Commun. *10*, 1251–1320.

STAR★METHODS

KEY RESOURCES TABLE

REAGENT or RESOURCE	SOURCE	IDENTIFIER
Antibodies		
anti-CMTR1	Atlas antibodies	Cat. No. HPA029980
anti-IFIT1	Cell signaling	Cat. No. D2X9Z
anti-TUBULIN	Abcam	Cat. No. ab6046
anti-PARK7	Abcam	Cat. No. ab18257
Rabbit anti-Mouse IgG (H + L) Superclonal™ Secondary Antibody, HRP conjugate	Invitrogen	Cat. No. A27025
Amersham ECL Rabbit IgG, HRP-linked whole Ab (from donkey)	GE Healthcare	Cat. No. NA934-1ML
Bacterial and virus strains		
Top10	N/A	N/A
Biological samples		
pACEBac2SS-hDHX15	This study	6xHis-Strep-SUMO-TEV- tags on protein
pIDK vector-hCMTR1	This study	https://www.snapgene.com/plasmids/insect_cell_vectors/pIDK
pACEBac2SS-hDHX15-hCMTR1	This study	Tagged DHX15 and untagged CMTR1
pACEBac2SS-hCMTR2(15–759 aa)	This study	6xHis-Strep-SUMO-TEV- tags on protein
Chemicals, peptides, and recombinant proteins		
Sodium deoxycholate	Sigma	Cat. No. 30968
Complete EDTA-free protease inhibitor	Roche	Cat. No. 11 873 580 001
TRIzol™ Reagent	Invitrogen	Cat. No. 15596-026
Trypan blue	Sigma	Cat. No. 93595-50ML
Propidium Iodide	Sigma	Cat. No. P4170
Ponceau S	Sigma	P3504
IMDM Medium	Gibco	Cat. No. 12440046
Dulbecco's modified Eagle Medium	Invitrogen	Cat. No. 21969-035
fetal bovine serum	ThermoFisher	Cat. No. 10270106
Penicilline/Streptomycin	ThermoFisher	Cat. No. 15140122
Glutamine	ThermoFisher	Cat. No. 25030024
Trypsin-EDTA 0.05%	ThermoFisher	Cat. No. 25300-054
Propidium Iodide	Sigma	Cat. No. P4170
30% acrylamide (37.5:1)	National Diagnostic	Cat. No. EC-890
N,N,N′,N′-Tetramethylethylendiamin	Merck	Cat. No. 1107320100
Tween 20	SIGMA	Cat. No. P7949
Amersham Prime Western Blotting Detection Reagen	GE Healthcare	Cat. No. RPN2232
SuperSignal West Femto Maximum Sensitivity Substrate	ThermoFisher	Cat. No. 34095
Pierce ECL 2 Substrate	ThermoFisher	Cat. No. 1896433A
Phire Green Hot Start II PCR Master Mix	Thermo Scientific	Cat. No. F126L
RNA Ligase 2	NEB	Cat. No.M0242S
RNAlater reagent	Invitrogen	Cat. No. AM7021
SUPERaseIn RNase inhibitor	Ambion	Cat. No. AM2694
RNase A	Sigma	R6513
Fetal Bovine serum	Gibco	Cat. No. 10270

(*Continued on next page*)

Continued

REAGENT or RESOURCE	SOURCE	IDENTIFIER
RNAse I	RNAse I	Cat. No. AM2295
Washing buffer B	Thermo Scientific	11900D
Critical commercial assays		
MinElute Gel Extraction Kit	Qiagen	Cat. No. 28604
Dynabeads™ Oligo(dT)25	ThermoFisher	Cat. No. 61005
RiboCop rRNA Depletion Kit V2 H/M/R	Lexogen	Cat. No. 144
RNA Clean and Concentrator kit	Zymo Research	Cat. No. R1017
AllPrep DNA/RNA/Protein Mini Kit	Qiagen	ID: 80004
DC Protein Assay (Bio-Rad, Cat. No. 5000112)	DC Protein Assay (Bio-Rad, Cat. No. 5000112)	DC Protein Assay (Bio-Rad, Cat. No. 5000112)
Deposited data		
Deep sequencing datasets	This study	GEO: GSE235348
All raw gel data will be deposited at Mendeley Data.	This study	https://doi.org/10.17632/rv9kgtcjpv.1
Experimental models: Cell lines		
Hap1 cells	Horizon Discovery	Cat. No. C631
Hap1 *CMTR1* KO cells	Horizon Discovery	Cat. No. HZGHC004217c007
Experimental models: Organisms/strains		
Mouse: *Cmtr1* knockout	The Jackson Laboratory	Stock no. 46174-JAX
Mouse: *Cmtr2 knockout*	MMRRC, UC Davis	Stock no. 047142-UCD
Mouse: *Cmtr1* floxed mouse	This study	Available from lead contact
Mouse: *AlbCreERT2*	Gift from David Gatfield lab	Schuler et al.[56]
Mouse: *Vasa-Cre*	Jackson Laboratory	Stock no. 6954
Oligonucleotides		
DNA and RNA oligos		See Table S1
Software and algorithms		
ENRICHR	Chen et al.[57]; Kuleshov et al.[58]	http://amp.pharm.mssm.edu/Enrichr/
R	R Core Team[59]	https://www.r-project.org
DESeq2	Love et al.[60]	N/A
Bioconductor	Huber et al.[61]	https://www.bioconductor.org/
Salmon	Patro et al.[62]	N/A
FastQC	Andrews[63]	N/A
Flexbar	Dodt et al.[64]	N/A
STAR	Dobin et al.[65]	N/A
Python 3.10.6		N/A
seaborn (v0.12.1)	Waskom[66]	https://doi.org/10.21105/joss.03021
matplotlib (v3.6.2)	Hunter[67]	N/A
gseapy (v0.14.0)	Fang et al.[68]	https://doi.org/10.1093/bioinformatics/btac757
bowtie	Langmead et al.[69]	N/A
CollectRnaSeqMetrics	Toolkit[70]	N/A
RiboCode toolkit	Xiao et al.[71]	N/A
SparK (v2.6.2) python library	Kurtenbach and Harbor[72]	N/A
SUPPA2	Trincado et al.[73]	N/A
SCDC (v0.0.0.9000) R package	Dong et al.[74]	N/A
sva (v3.46.0) bioconductor package	Leek et al.[75]	N/A
plastid python package	Dunn and Weissman[76]	N/A
sklearn (v1.1.3)	Pedregosa et al.[77]	N/A
Kaluza software	Beckman	RRID:SCR_016182

(*Continued on next page*)

Continued

REAGENT or RESOURCE	SOURCE	IDENTIFIER
Other		
Amersham Hyperfilm ECL	GE Healthcare	Cat. No. 28906837
Amersham Protran 0.45 μm nitrocellulose membrane	GE Healthcare	Cat. No. 10600002

RESOURCE AVAILABILITY

Lead contact

Further information and requests for resources and reagents should be directed to and will be fulfilled by the lead contact, Ramesh S. Pillai (ramesh.pillai@unige.ch).

Materials availability

All unique reagents generated in this study are available from the lead contact without any restriction. The *Cmtr1* knockout mouse (MMRRC Stock No. 46174-JAX) was obtained from The Jackson Laboratory, while the *Cmtr2* knockout mouse (MMRRC Stock No. 047142-UCD) was from the MMRRC, UC Davis. The *Ddx4-Cre* (*Vasa-Cre*) transgenic line was obtained from the Jackson Laboratory (Jackson Laboratory, Stock no. 6954). And the Alb-CreERT2 mouse was a gift from David Gatfield, University of Lausanne, Switzerland. The HAP1 *CMTR1* knockout cell line (Horizon Discovery, Cat. No. HZGHC004217c007) and control wildtype cells (Horizon Discovery, Cat. No. C631) were purchased.

Data and code availability

- Deep sequencing data generated in this study are deposited with Gene Expression Omnibus (GEO) under accession no. GEO: GSE235348
- Code used in the current study is available from the lead contact upon reasonable request.
- Other raw data associated with this study are deposited with Mendeley Data (https://doi.org/10.17632/rv9kgtcjpv.1).

EXPERIMENTAL MODEL AND STUDY PARTICIPANT DETAILS

Animal work

The *Cmtr1* floxed mouse was generated at the Transgenic Mouse Facility of University of Geneva, while the *Cmtr1* and *Cmtr2* knockout models were generated by the Knockout Mouse Project (KOMP). Mice were bred in the Animal Facility of Sciences III, University of Geneva. The use of animals in research at the University of Geneva is regulated by the Animal Welfare Federal Law (LPA 2005), the Animal Welfare Ordinance (OPAn 2008) and the Animal Experimentation Ordinance (OEXA 2010). The Swiss legislation respects the Directive 2010/63/EU of the European Union. Any project involving animals has to be approved by the Direction Générale de la Santé and the official ethics committee of the Canton of Geneva, performing a harm-benefit analysis of the project. Animals are treated with respect based on the 3Rs principle in the animal care facility of the University of Geneva. We use the lowest number of animals needed to conduct our specific research project. Discomfort, distress, pain and injury is limited to what is indispensable and anesthesia and analgesia is provided when necessary. Daily care and maintenance are ensured by fully trained and certified staff. Animals were maintained in ventilated cages with unrestricted supply of water and food. All adult experimental animals were sacrificed by intraperitoneal injection of 150 mg/kg pentobarbital followed by the cervical dislocation, while decapitation was used for P0 animals. This work was approved by the Canton of Geneva (GE/16/219C and GE297).

Mouse mutants

The *Cmtr1* (C57BL/6NJ-*Cmtr1*$^{em1(IMPC)J}$/Mmjax) knockout mouse was purchased from The Jackson Laboratory (strain # 032957; MMRRC Stock no. 46174-JAX). The heterozygous mutant animals obtained from the Jackson Laboratory (via Charles River) were crossed with wildtype C57BL/6J (Janvier; stock no. SC-C57J-F; SC-C57J-M) partners to expand the colony.

The *Cmtr2* mutant mouse (C57BL/6N-*Cmtr2*$^{tm1.1(KOMP)Vlcg}$/JMmucd, MMRRC_047142-UCD, Stock no. 047142-UCD) was generated by the Knockout Mouse Phenotyping Program (KOMP) Repository, and obtained from the Mutant Mouse Resource and Research Center (MMRRC), University of California at Davis. We crossed the heterozygous mutant animals obtained from the UC Davis with wildtype C57BL/6J (Janvier; stock no. SC-C57J-F; SC-C57J-M) partners to expand the colony.

We created *Cmtr1* conditional knockout mice by knock-in of *loxP* sites in the same direction (recombination by the Cre recombinase should result in deletion of the intervening region) flanking the exon 3 of *Cmtr1* (Figure S2A). Founder mice were crossed with wildtype C57BL/6J (Janvier) partners to obtain germline transmission. Homozygous *Cmtr1*$^{loxP/loxP}$ animals are viable and fertile.

We prepared the conditional knockouts (cKO) (*Cmtr1*$^{loxP/-}$; *Alb-CreERT2*$^{KI/+}$ mice) and control (*Cmtr1*$^{loxP/+}$; *Alb-CreERT2*$^{KI/+}$) animals to delete the gene in mouse liver. Animals (n = 4) were intraperitoneally injected with Tamoxifen (75 μg/g of body weight) to

induce gene deletion in adult animals: 3 months-old (for day 2 experiment), 4 months-old (for day 6 experiment) and 8 months-old (for day 22 experiment) (Figure 3E, 3H, and 3I). We did these experiments in two batches. The first batch had only one time point (day2: 4 days of injection and analysis at day 2 post-tamoxifen injection) (Figures 3C–3G and 3J–3M) with control and conditional KO liver samples. To observe the chronic effects of loss of *Cmtr1*, we performed a second experiment with three time-points (day 2, 6 and 22) (GO term analysis in Figure S3C and volcano plots in Figures 3H and 3I) with control and conditional KO liver samples for each time point. At least three biological replicates were used for each time point (Table S2). Ribosome profiling (n = 4) was done with the first batch of liver samples from the day 2 time point. Sucrose-gradient analysis to obtain the polysome profiling data was conducted in duplicates only (Figures 3K and S3D).

The *Ddx4-Cre* (*Vasa-Cre*) transgenic line (Jackson Laboratory, Stock no. 6954) expresses the Cre recombinase from the *Ddx4* (*Vasa*) promoter.[78] We crossed $Cmtr1^{loxP/loxP}$ animals with $Cmtr1^{+/-}$;$Ddx4^{KI/+}$ mice to prepare the conditional knockouts (cKO) ($Cmtr1^{loxP/-}$; $Ddx4^{KI/+}$) and control animals ($Cmtr1^{loxP/+}$; $Ddx4^{KI/+}$). The testes (P0, P31 and P75) and ovaries (>P60) from cKO and control animals of the indicated ages were collected for histological and/or transcriptome analysis.

Mouse embryos (E6.5, E7.5 etc) were microdissected, imaged using stereomicroscope Discovery.V12 (Zeiss), and stored in RNA-later reagent (Invitrogen, Cat. No. AM7021) until RNA extraction. Samples were washed 3 times in ice-cold 1xPBS prior the RNA and DNA extraction by the AllPrep DNA/RNA/Protein Mini Kit (Qiagen, Cat. No./ID: 80004) and genotyped as described above.

Human HAP1 *CMTR1* KO cells

HAP1 is a near-haploid human cell line derived from the chronic myelogenous leukemia (CML) cell line KBM-7. The HAP1 *CMTR1* knockout cell line (Horizon Discovery, Cat. No. HZGHC004217c007) and control wildtype cells (Horizon Discovery, Cat. No. C631) were purchased. The *CMTR1* KO cell line has a 2 bp deletion in the target locus and was generated using the CRISPR-Cas9 technology. Western analysis confirms the complete lack of CMTR1 protein (Figure S4A) and RNA mass spectrometry reveals the complete absence of m^6Am (Figure S4B), a modification that depends on CMTR1-dependent cap1 methylation.[11]

METHOD DETAILS

Cmtr1 knockout mouse

The *Cmtr1* (C57BL/6NJ-$Cmtr1^{em1(IMPC)J}$/Mmjax) knockout mouse was purchased from The Jackson Laboratory (strain # 032957; MMRRC Stock no. 46174-JAX). It was generated by the Knockout Mouse Phenotyping Program (KOMP) at the Jackson Laboratory. The mouse *Cmtr1* gene locus on Chromosome 17 (NCBI: NM_028791) has 24 exons. The mutant was prepared by electroporation of two gRNAs (GCAGGACCCACACTAGACAT and GGTGGGGCACAAGTTAGCAC) targeting intronic regions flanking the exon 3 of the *Cmtr1* gene (Figure S1A). The guide RNAs and Cas9 endonuclease were introduced into single mouse embryos (C57BL/6NJ; The Jackson Laboratory Stock No. 5304). This makes a 344 bp deletion beginning at Chromosome 17 position 29,674,049 bp and ending after 29,674,392 bp (GRCm38/mm10). This deletes the entire exon 3 and 192 bp of flanking intronic sequence (Figure S1A). The heterozygous mutant animals obtained from the Jackson Laboratory (via Charles River) were crossed with wildtype C57BL/6J (Janvier; stock no. SC-C57J-F; SC-C57J-M) partners to expand the colony.

Cmtr2 knockout mouse

The *Cmtr2* mutant mouse (C57BL/6N-$Cmtr2^{tm1.1(KOMP)Vlcg}$/JMmucd, MMRRC_047142-UCD, Stock no. 047142-UCD) was generated by the Knockout Mouse Phenotyping Program (KOMP) Repository, and obtained from the Mutant Mouse Resource and Research Center (MMRRC), University of California at Davis. The mouse *Cmtr2* gene locus on Chromosome 8 has two exons, with the protein encoded by sequences in the exon 2. The mutant mice were created (Velocigene) by a targeted mutation of the locus via homologous recombination in mouse embryonic stem (ES) cells (VGB6 derived from C57BL/6NTac). This results in deletion of 2311 bp that includes the whole mouse CMTR2 coding sequence in exon 2 (mm10, chr8: 110,221,063–110,223,373 is deleted), and insertion of a cassette (*LacZ-loxP-Neo-loxP*) in its place (http://velocigene.com/komp/detail/15502) (Figure S5A). Such a *Cmtr2* knockout ES cell clone (15502A-C9) was injected into morulae or blastocysts. Resulting chimera founders were mated to C57BL/6N mice to obtain germline transmission. The obtained heterozygous animals were then bred to a ubiquitous Cre deleter mouse line for recombination of the *LoxP* sites to remove the *Neo* gene from the inserted cassette by Cre recombinase. The end result is that the *Cmtr2* knockout mouse lacks the CMTR2 coding sequence, leaving the *LacZ* coding sequence under control of the endogenous *Cmtr2* promoter. The Cre transgene was removed during the crosses. The MMRRC used C57BL/6N females for cryo-recovery. We crossed the heterozygous mutant animals obtained from the UC Davis with wildtype C57BL/6J (Janvier; stock no. SC-C57J-F; SC-C57J-M) partners to expand the colony.

Creation of *Cmtr1 loxP* mice

The *Cmtr1* genomic locus is located on mouse chromosome 17 and consist of 23 exons. We created *Cmtr1* conditional knockout mice by knock-in of *loxP* sites in the same direction (recombination by the Cre recombinase should result in deletion of the intervening region) flanking the exon 3 of *Cmtr1* (Figure S2A). The ssDNA had a central region with two *loxP* sites at positions 85 nt upstream and

55 nt downstream of exon 3, with 70nt homology arms at each end. We introduced mutations into the ssDNA to prevent repeat cleavage of the target sites: the upstream gRNA recognition site is disrupted by insertion of the *loxP* site, while we mutated the PAM sequence at the downstream site.

The tracrRNA and crRNAs (crRNA_Cmtr1_1 and crRNA_Cmtr1_2) (IDT) (Table S1) were annealed in thermocycler in two separate reactions: 2 μL tracrRNA (200 pmol; IDT; Cat. No. 1072533) and 2 μL crRNA (200 pmol; IDT) (Table S1) were mixed with 6 μL IDTE buffer (pH 7.5; IDT, Cat. No. 356429). Annealed gRNAs were stored at −70°C. The injection mix was prepared freshly on the day of mouse oocyte injections. The annealed gRNAs (to final concentration 0.6 pmol/μL) were mixed with the pre-diluted Cas9 3xNLS protein (to final concentration 30 ng/μL; IDT, Cat. No. 1081058) in a volume of 9 μL. The mix was incubated at room temperature for 10 min for complex formation and mixed with the ssDNA repair template (Genewiz; 10 ng/μL final concentration). The volume of this injection mix was adjusted with the IDTE buffer to a final volume of 100 μL. The injection mix was centrifuged at 13000 rpm for 5 min at 4°C, and 50 μL of supernatant was transferred to a new microcentrifuge tube and stored on ice. Mouse single-cell embryos of the B6D2F1/J hybrid line (also called B6D2; The Jackson Laboratory, stock no. 100006) were injected. The NMRI (Naval Medical Research Institute) mice, which have a white coat color, were used as foster mothers. Founder mice were identified by genotyping PCR and crossed with wildtype C57BL/6J (Janvier) partners to obtain germline transmission. Homozygous *Cmtr1*$^{loxP/loxP}$ animals are viable and fertile.

ssDNA repair template:

gRNAs are in italics, bold underlined are *loxP* sites insertions, in bold exon3, "A" in bold upstream of gRNA is a mutation in PAM sequence to avoid multiple cleavages.

ATACGTACGTATACAGCTGGCAAGAGTAGAGACGTCACTGTGACCTCCATTGAGTGCAGGACCC*ACACTA***ATAACTTCGTATAG**
CATACATTATACGAAGTTAT*GACATAGGTGGGAC*ATGTGGACTGTGGGTGCATGAGGCAGTCCTGTCATCCGGACCCACCTAACG
CTTCTCTTCTTCTTCCCCAG**CATCTGCTACAAGCCTCAGTGGATCTGACAGTGAGACCGAGGGGAAGCAGCCCTGCTCTGATGA**
TTTCAAAGATGCCTTCAAAGCAGATTCCCTTGTGGAGGGAACATCGTCCCGATATTCCATGTATAACAGTGTTTCCCAGAGGCT
TATGGTATGTCTTGGCTTAGAATGGACTTCTAAAGTTGCCCAAAAGAGGGAGAGGAAGA**ATAACTTCGTATAGCATACATTATACGA**
AGTTATGGGC**A***AGGGTGTACTGGTGTTGGGGA*GTGGGGTGGGGCACAAGTTAGCACAGGATATAGGTTCTGAGTAT.

Tamoxifen-inducible conditional *Cmtr1* deletion in mouse liver

The Alb-CreERT2 mouse[56] specifically expresses using the *Albumin* (Alb) promoter the tamoxifen-inducible CreERT2 in hepatocytes. As described by the authors,[56] a cassette consisting of an IRES with coding sequence for Cre-ERT2 was inserted (knock-in) downstream of the stop codon, in the 3′ UTR of the serum albumin (Alb) gene. The Alb-CreERT2 mouse was a gift from David Gatfield, University of Lausanne, Switzerland. The *Cmtr1*$^{loxP/loxP}$ mice were crossed with *Alb-CreERT2*$^{KI/KI}$ mice. In another cross, the *Cmtr1*$^{+/-}$ mice were crossed with the *Alb-CreERT2*$^{KI/KI}$ mice. Using the these lines we prepared the conditional knockouts (cKO) (*Cmtr1*$^{loxP/-}$; *Alb-CreERT2*$^{KI/+}$ mice) and control (*Cmtr1*$^{loxP/+}$; *Alb-CreERT2*$^{KI/+}$) animals. Animals (n = 4) were intraperitoneally injected with Tamoxifen (75 μg/g of body weight) to induce gene deletion in adult animals: 3 months-old (for day 2 experiment), 4 months-old (for day 6 experiment) and 8 months-old (for day 22 experiment) (Figures 3E, 3H, and 3I).

We did these experiments in two batches. The first batch had only one time point (day2: 4 days of injection and analysis at day 2 post-tamoxifen injection) (Figures 3C–3G and 3J–3M) with control and conditional KO liver samples. To observe the chronic effects of loss of *Cmtr1*, we performed a second experiment with three time-points (day 2, 6 and 22) (GO term analysis in Figure S3C and volcano plots in Figures 3H and 3I) with control and conditional KO liver samples for each time point. At least three biological replicates were used for each time point (Table S2). Ribosome profiling (n = 4) was done with the first batch of liver samples from the day 2 time point. Sucrose-gradient analysis to obtain the polysome profiling data was conducted in duplicates only (Figures 3K and S3D).

Tamoxifen (Sigma, Cat. No. T5648-1G) was diluted in corn oil (Sigma, Cat. No. C8267-500ML) and dissolved overnight at room temperature, protected from light, and stored at 4°C for up to 2 days. Daily injections of tamoxifen were given for four consecutive days after which the mice were sacrificed at different time points: 2 days later (6 days after start of the experiment); 6 days later (10 after start of the experiment) or 22 days later (26 after start of the experiment). After injections, the animals were monitored daily for change in body weight, signs of general discomfort and behavior changes. We observed total loss of the CMTR1 protein already at 2 days-post tamoxifen injections (Figure 3C), but the longer analysis time-points were used to detect long-term gene expression consequences of loss of the protein. By analysis of the transcriptome at the three time-points, chronic activation of the innate immune pathway was observed in the cKO *Cmtr1* liver tissue (Figures 3E, 3H, and 3I). Animals were euthanized by pentobarbital injection followed by cervical dislocation and livers were collected.

Conditional *Cmtr1* germline knockout mice

The *Ddx4-Cre* (*Vasa-Cre*) transgenic line (Jackson Laboratory, Stock no. 6954) expresses the Cre recombinase from the *Ddx4* (*Vasa*) promoter.[78] There are multiple copies of this transgene in this line. The obtained animals were first twice backcrossed with wildtype C57BL/6J prior to other crosses. We crossed *Cmtr1*$^{loxP/loxP}$ animals with *Cmtr1*$^{+/-}$;*Ddx4*$^{KI/+}$ mice to prepare the conditional knockouts (cKO) (*Cmtr1*$^{loxP/-}$; *Ddx4*$^{KI/+}$) and control animals (*Cmtr1*$^{loxP/+}$; *Ddx4*$^{KI/+}$). The testes (P0, P31 and P75) and ovaries (>P60) from cKO and control animals of the indicated ages were collected for histological and/or transcriptome analysis. Expression of the Cre recombinase starts at embryonic day 14.5 (E14.5) in the male and female germline. Meiosis is initiated at E13.5 in the female germline, and at P8 in the male germline. The cKO males were found to be infertile, while cKO females displayed low penetrant infertility

(Figures 2B–2E). We speculate that deletion of *Cmtr1* after initiation of meiosis in the female germline may be the reason for the not dramatically affect progression of oogenesis.

Mouse genotyping

Ear-punches of the weaned animals (21 days-old) were digested in 100 μL of Lysis buffer (10 mM NaOH, 0.1 mM EDTA) for 90 min at 95°C. After centrifugation at 3000 rcf for 10 min, 50 μL of the supernatant was transferred to a new tube containing 50 μL of TE buffer (20 mM Tris-HCl, pH 8.0 and 0.1 mM EDTA). An aliquot of 2 μL of the digestion mix was used for the genotyping PCR. Reaction mix for 20 μL PCR reactions: 10 μL of Phire Green Hot Start II PCR Master Mix (Thermo Scientific, Cat. No. F126L), 1.0 μL of each primer (10 nM), 2.0 μL DNA from ear punches (100–200 ng), and 5–6.0 μL water to make 20 μL final volume.

Primers to genotype knockout allele of *Cmtr1* were RR1185 and RR1186 (Table S1). The expected size of products was 916 bp (WT) and 661 bp (KO). Reactions were run using the following conditions: 98°C for 30 s, 35 cycles of [98°C for 5 s, 65°C for 5 s and 72°C for 12 s], 72°C for 1 min, and finally at 12°C to hold the reaction. Reactions were examined by 1.5% agarose gel electrophoresis (Figure S1B).

To identify knockout allele of *Cmtr2*, PCR reaction with three primers (MD280, MD282, MD283) were used (Table S1). Reactions were run using the following conditions: 98°C for 30 s, 35 cycles of [98°C for 5 s, 65°C for 5 s and 72°C for 12 s], 72°C for 1 min, and finally at 12°C to hold the reaction. PCR products of 244 bp (WT) and 339 bp (KO) were resolved by 2% agarose gel electrophoresis (Figure S5B).

To genotype *Cmtr1 LoxP* allele, the primers were MM458 and MM448 with the expected PCR product size 408 bp (WT) and 476 (KI) (Table S1). Reactions were run using the following conditions: 98°C for 30 s, 35 cycles of [98°C for 5 s, 65°C for 5 s and 72°C for 12 s], 72°C for 1 min, and finally at 12°C. Reactions were examined by 2% agarose gel electrophoresis (Figure S2B and S3A).

To genotype *DDX4* transgene, the primers were MM113 and MM114 with the expected PCR product size for the transgene fragment being 275 bp (Table S1). Reactions were run using the following conditions: 98°C for 30 s, 35 cycles of [98°C for 5 s, 65°C for 5 s and 72°C for 12 s], 72°C for 1 min, and finally at 12°C. Reactions were examined by 2% agarose gel electrophoresis (Figure S2B).

In case of the *Alb-CreERT2* animals, the WT allele was screened with ABT290 and ABV93 primers (Table S1), whereas the KI allele was detected with ABT290 and ABT294 in two different reactions with the following reaction conditions: 98°C for 30 s, 35 cycles of [98°C for 5 s, 55°C for 5 s and 72°C for 12 s], 72°C for 1 min, and finally at 12°C. PCR products were mixed together and examined by 2% agarose gel electrophoresis, where 444 bp (KI) and 229 bp (WT) bands were detected (Figure S3A).

Collection of mouse embryos

Adult (8 weeks or older) animals of the heterozygous genotypes for *Cmtr1* or *Cmtr2* knockout alleles were crossed together. Plugs were checked the morning after and considered as embryonic day 0.5 (E0.5). Plugged females were separated and sacrificed later at E6.5 to E10.5. Embryos were microdissected, imaged using stereomicroscope Discovery.V12 (Zeiss), and stored in RNAlater reagent (Invitrogen, Cat. No. AM7021) until RNA extraction. Samples were washed 3 times in ice-cold 1xPBS prior the RNA and DNA extraction by the AllPrep DNA/RNA/Protein Mini Kit (Qiagen, Cat. No./ID: 80004) and genotyped as described above.

Human HAP1 *CMTR1* KO cells

HAP1 is a near-haploid human cell line derived from the chronic myelogenous leukemia (CML) cell line KBM-7. The HAP1 *CMTR1* knockout cell line (Horizon Discovery, Cat. No. HZGHC004217c007) and control wildtype cells (Horizon Discovery, Cat. No. C631) were purchased. The *CMTR1* KO cell line has a 2 bp deletion in the target locus and was generated using the CRISPR-Cas9 technology. Western analysis confirms the complete lack of CMTR1 protein (Figure S4A) and RNA mass spectrometry reveals the complete absence of m^6Am (Figure S4B), a modification that depends on CMTR1-dependent cap1 methylation.[11]

Clones and constructs

The complementary DNA (cDNA) for human CMTR1 (NCBI: NP_055865.1), human DHX15 (NCBI: NP_001349.2) and mouse CMTR2 (NCBI: NP_666327.2) were obtained by reverse transcription-PCR (RT-PCR) amplification from human cell culture or mouse tissue RNA. To express the protein in insect cell expression system, full-length hCMTR1, hDHX15 or truncated mCMTR2 (15–759 aa) coding sequence was cloned into the modified pACEBac2SS vector for expression as an N-terminal 6xHis-Strep-SUMO-TEV fusion protein. For co-expression of hCMTR1 and hDHX15, hCMTR1 coding sequence was cloned into pIDK vector and then recombined with pACEBac2SS-hDHX15 via Cre-recombination. All constructs were verified by restricted digestion as well as by Sanger sequencing.

Recombinant protein production

Production of full-length hCMTR1, hDHX15 or truncated mCMTR2 was carried out in insect cell lines using the baculovirus expression system. The ovary-derived cell lines used are: High Five (Hi5) insect cell line originating from the cabbage looper (*Trichoplusia ni*) and the *Sf*9 cells derived from the fall army worm *Spodoptera frugiperda*. Briefly, pACEBac2SS plasmids carrying target genes were transformed into DH10EMBacY competent cells for recombination with the baculovirus genomic DNA (bacmid). The bacmid DNA was extracted and transfected with FuGENE HD (Promega, cat. no. E231A) into the *Sf*9 insect cells for virus production. The supernatant (V_0) containing the recombinant baculovirus was collected after 72 to 96 h post-transfection. To expand the virus pool, 3.0 mL of the V_0 virus stock was added into 25 mL of *Sf*9 (0.5×10^6/mL) cells. The resulting cell culture supernatant (V_1) was collected 24 h

post-proliferation arrest. For large-scale expression of the protein, Hi5 cells were infected with virus (V_1) and cells were harvested 72 h after infection. For expression of the CMTR1-DHX15 complex, recombined plasmid carrying both CMTR1 and DHX15 gene was transformed into DH10EMBacY competent cells, followed by bacmid extraction and baculovirus preparation as described above.

Purification of mouse CMTR2 protein

After protein expression, the cells were collected by centrifugation and lysed by sonication in buffer: 50 mM Tris-HCl, pH 8.0, 300 mM NaCl, 5% Glycerol, 5 mM 2-mercaptoethanol, 40 mM Imidazole and protease inhibitor (Thermo Scientific, EDTA-free). Clear supernatant was collected by centrifugation at 18,000 rpm for 45 min at 4°C. The supernatant was incubated for 2 h with Ni^{2+} chelating Sepharose FF beads at 4°C, then the beads were washed by imidazole gradient washing buffer and finally bound protein was eluted with 250 mM imidazole in lysis buffer. Subsequently, the N-terminal tag was cleaved by the TEV protease overnight in the dialysis buffer (50 mM Tris-HCl pH 8.0, 300 mM NaCl, 5 mM 2-mercaptoethanol). The cleaved tag was removed by a second purification on Nickel beads. The protein was further purified by gel filtration chromatography (GE Healthcare, Superdex 200 increase 10/300) equilibrated with buffer (25 mM Tris-HCl pH 8.0, 150 mM KCl, 5% glycerol and 1 mM DTT). The pure fractions were verified by SDS-PAGE electrophoresis and flash-frozen in liquid nitrogen.

Purification of human CMTR1-DHX15 complex

Hi5 cells co-expressing untagged hCMTR1 and 6xHis-Strep-SUMO-TEV-hDXH15 were collected and resuspended in lysis buffer (50 mM Tris-HCl pH 8.0, 300 mM NaCl, 40 mM Imidazole, 5% glycerol and 5 mM 2-mercaptoethanol) supplemented with protease inhibitor (Thermo Scientific, EDTA-free). After sonication, the lysate was centrifuged at 18,000 rpm for 45 min at 4°C. The clarified supernatant was incubated at 4°C for 2h with the Ni^{2+} chelating Sepharose FF beads. The beads were washed with an imidazole gradient in the wash buffer (40 mM, 50 mM or 60 mM imidazole in lysis buffer) and bound protein complex was eluted by 250 mM Imidazole. The N-terminal His-Strep-SUMO tag was further removed by TEV protease overnight at 4°C in dialysis buffer (50 mM Tris-HCl pH 8.0, 200 mM NaCl, 5 mM 2-mercaptoethanol). After cleavage, second nickel column purification was performed and flow-through containing the cleaved protein (complex) was collected. The complex was further purified by gel filtration chromatography using Superdex 200 increase 10/300 (GE Healthcare) equilibrated with buffer (25 mM Tris-HCl pH 8.0, 150 mM KCl, 5% glycerol and 1 mM DTT). The pure fractions were verified by SDS-PAGE electrophoresis (Figure S4J) and flash-frozen in liquid nitrogen.

Antibodies

Commercial antibodies

Primary antibodies: rabbit or mouse anti-CMTR1 (Atlas antibodies, Cat. No. HPA029980), anti-IFIT1 (Cell signaling, Cat. No. D2X9Z), rabbit anti-TUBULIN (abcam, Cat. No. ab6046) and rabbit anti-PARK7 (abcam, Cat. No. ab18257).

Secondary antibodies: For Western blot analyses, the following secondary antibodies conjugated to HorseRadish Peroxidase were used: Amersham ECL Rabbit IgG, HRP-linked whole Ab (from donkey) (Cat. No. GE Healthcare, NA934-1ML) and Rabbit anti-Mouse IgG (H + L) Superclonal Secondary Antibody, HRP conjugate (Invitrogen, Cat. No. A27025).

Antibodies generated for this study

We generated rabbit polyclonal antibodies to mouse CMTR2 (mCMTR2). Two New Zealand White (NZW) rabbits were immunized with the soluble antigen (Biotem, France). The antigen used was the purified untagged mouse CMTR2 (15–759 aa) produced in insect cells. For each injection, 1 mg/mL protein was used. After six injections (at day 0, 14, 28, 56, 70 and 89) crude immune serum was collected (at day 96) and frozen. The anti-mCMTR2 crude sera detected the recombinant mouse protein by Western analysis, but failed to detect the protein in mouse tissue lysates. This could be due to low abundance of CMTR2 in mouse tissues or due to the low titer of the antibodies generated. Affinity purification of the antibodies with the antigen did not help to improve the situation.

Collection of RNA from HAP1 cells

Wildtype and *CMTR1* knockout human HAP1 cells were cultured in (High glucose) IMDM Medium (Gibco, Cat. No. 12440046) supplemented with 10% fetal bovine serum (FBS) and Penicillin-Streptomycin (10,000 U/mL) 1:100 (Gibco, Cat. No. 15140122) at 37°C in the presence of 5% CO2. At 70% confluency, the media was removed and TRIzol Reagent (Invitrogen, Cat. No. 15596-026) was added to monolayer of cells. Mixture was collected to a micro centrifuge tube, flash frozen and stored at −70°C until the RNA extraction.

RNA extraction from cell lines

After harvesting, pellets of human HAP1 cells were directly mixed with the TRIzol reagent (Invitrogen, Cat. No. 15596026), flash frozen and kept at −70°C. They were then processed according to the manufacture's protocol. To remove genomic DNA, approximately 10 μg of the extracted RNA was treated with TurboDNase (Invitrogen, Cat. No. AM2238) for 30 min and then cleaned by RNA Clean and Concentrator kit (Zymo Research, Cat. No. R1017).

Growth curve

We seeded 0.5 million wildtype or *CMTR1* knockout human HAP1 cells into wells of a 12-well plate and for the next 4 days cells were collected daily by trypsinization and counted in duplicate by Countess 3 Automated cell (Invitrogen) counter in trypan blue (Sigma, Cat. No. 93595-50ML) mixture 1:1. This experiment was repeated six times to obtain the data presented (Figure S4C).

Analysis of cell cycle by FACS

Wildtype and *CMTR1* knockout human HAP1 cells were grown to 60–70% confluency and then collected by trypsinization. Cell suspension was centrifuged at 500xg for 5 min, followed by removal of the trypsin/media. Cells were washed once in 1xPBS and centrifuged again. The PBS was removed and cells were completely resuspended in 100 μL of ice-cold 1xPBS. Afterward, cells were fixed by addition of ice-cold 100% Methanol, mixed and stored at −20°C until staining and further analysis. Later, fixed cells were centrifuged at 500xg at 4°C for 10 min. Supernatant was removed and cells were permeabilized with 150 μL PBS with 0.2% Triton X- and incubated for 30 min at room temperature. Cells were centrifuged, supernatant removed, and cells were resuspended in 500 μL of staining solution [15 μg/mL Propidium Iodide (Sigma, Cat. N P4170) and 6 μg/mL RNase A (Sigma Cat. no. R6513)]. Staining was performed for at least 1H in dark at 4°C. FACS analysis was performed in the staining solution using Gallios Flow Cytometer (Beckman) and analyzed by Kaluza software (Figure S4D).

Collecting mouse tissues for western blot

Multiple tissues were isolated from an adult (>P60) mouse. After flash-freezing in liquid nitrogen, a piece of different tissues were omogenized in 1 mL lysis buffer [50 mM Tris pH 7.4, 150 mM NaCl, 0.5% Triton X-100, 0.5% sodium deoxycholate, 1 mM DTT, Complete Protease Inhibitor Cocktail Tablet (Roche, Cat. No. 5056489001)]. The lysate was transferred to a 1.5 mL Eppendorf tube, centrifuged at 14000xg for 30 min, and the supernatant collected. An aliquot was taken to measure the concentration by DC Protein Assay (Bio-Rad, Cat. No. 5000112). Lysate concentrations were normalized to 1 mg/μL. Protein extracts were stored at −70°C. The SDS loading buffer was added to the protein lysates and boiled at 95°C for 5 min, and 30 μg of protein per lane was loaded and resolved by SDS-PAGE (Figure 3A).

Western Blot

Whole cell lysates or tissues were separated via SDS-PAGE in order to detect proteins of interest in 10% or 12% polyacrylamide gels. Gel electrophoresis was performed at 120 V for 110 min. After separation, proteins were blotted on the Amersham Protran 0.45 μm nitrocellulose membrane (GE Healthcare, Cat. No. 10600002) overnight at 5 V at room temperature using Trans-Blot SD Semi-Dry Transfer Cell system (Bio-Rad, Cat. No. 1703940). After transfer, membranes were washed with PBS and blocked for 1 h at room temperature with 5% dry milk in PBS with 0.05% Tween 20 (PBST) (Sigma, Cat. No. P7949). After this, membranes were incubated with primary antibody overnight at 4°C 1:10000 rabbit anti-TUBULIN (Abcam, Cat. No. ab6046), 1:100 anti-CMTR1 (Atlas antibodies, Cat. No. HPA029980), 1:200 anti-IFIT1 (Cell signaling, Cat. No. D2X9Z), 1:100 anti-PARK7 (abcam, Cat. No. ab18257). Then, membranes were washed 3 times for 10 min with PBST and incubated with HRP-conjugated secondary antibody at 1:10 000 dilution, either with anti-rabbit IgG HRP-linked (GE Healthcare, Cat. No. NA934) or anti-mouse IgG HRP-linked (Invitrogen, Cat. No. a27025) for 1 h at room temperature in 5% milk in PBST. After 1 h, membranes were washed 3 times for 10 min with PBST and incubated with one of detection reagents: Amersham Prime Western Blotting Detection Reagent (GE Healthcare, Cat. No. RPN2232), SuperSignal West Femto Maximum Sensitivity Substrate (ThermoFisher, Cat. No. 34095) or Pierce ECL 2 Substrate (ThermoFisher, Cat. No. 1896433A) for 5 min at room temperature. Signal was detected using Amersham Hyperfilm ECL (GE Healthcare, Cat. No. 28906837). The processed films were scanned using Perfection 3200 Photo scanner (Epson) with XSane image scanning software (ver. 0999).

Histological analysis of mouse tissues

To prepare the paraffin sections, the mouse tissues were washed in 1xPBS, and fixed in 4% paraformaldehyde overnight at 4°C. After washing in 1xPBS, samples were transferred into the embedding cassettes (Simport; cat. no. M508-3) and sent to the histology platform of University of Geneva. The samples were dehydrated in 70% ethanol (2 × 3h), 90% (1h), 95% (1h) and 100% ethanol (3 × 30 min) followed by incubation (3 × 30 min) in xylene. Xylene was removed and replaced with paraffin, and incubated at 56–58°C. Tissues were then transferred into plastic molds (Polysciences mold S-22; NC0397999) filled with paraffin, and paraffin was allowed to solidify at room temperature. The tissue sections (~5 μM thickness) were prepared using a microtome. The sections were allowed to stretch at 42°C and then stored at room temperature.

For histological analysis, the slides containing the paraffin sections were placed in a glass slide holder filled with xylene (3 × 5 min) to remove the paraffin. For rehydration, the slides were incubated in 100% ethanol, 96% ethanol, 70% ethanol, 50% ethanol (2 × 10 min for each step) and miliQ water (2 × 2 min for each step). Sections were stained with Hematoxylin solution (Merck) for 3 min and rinsed in running tap water. Then, sections were stained with Eosin Y solution (Sigma Aldrich; cat. no. E4382) for 3 to 5 min and washed with water. For dehydration, the sections were incubated in 50% (30 s), 70% (30 s), 96% (30 s), 100% ethanol (2 min) and HistoSAV (3 × 3 min). Neo-Mount (Merck) was put on the sections and immediately covered with coverslips. The sections were examined and pictures were taken using widefield (Zeiss Axio Imager Z1 or Axio M2) microscopy.

Total RNA purification from mouse liver samples

For total RNA extraction, we used multiple biological replicates (n = 4) of mouse liver from control (*Cmtr1*$^{loxP/+}$*; Alb-Cre-ERT2*) and *Cmtr1* cKO (*Cmtr1*$^{loxP/-}$*; Alb-Cre-ERT2*) animals after tamoxifen injections. Approximately 0.5 g tissue was taken and placed in a 50 mL conical tube (Sarstedt, Cat. No. 62.547.254) with 5 mL of extraction buffer. [Preparation of the extraction buffer: 250 g

guanidium thiocyanate (ITW Reagents, Cat. No. A1107), 17.6 mL sodium citrate, 0.75 M, pH 7.0 (Sigma-Aldrich, Cat. No. C8532) and 320 mL water were mixed at 60°C. Add 1/10 volume of sodium acetate, 2 M, pH 4.0 (Merck, Cat. No. 1.06268); 1/100 volume β-mercaptoethanol (Sigma, M3148), before use.]

Homogenize using a douncer (Kinematica AG, Cat. No. PT 2500E) in the 50 mL conical tube for 20 s until no fragments are left, and then add 5 mL phenol-H2O, mix well and stand on ice. Add 2 mL chloroform (VWR, Cat. No. 8.22265.2500): isoamyl alcohol (Merck, Cat. No. W205702) (49:1), mix well, stand on ice for 15 min, and transfer all the solution to a 15 mL TPP centrifuge tube (Thermo Fisher, Cat. No. 91016). Spin down for 20 min at 4000 rpm at 4°C, transfer the upper phase (approximately 5 mL) to a new 15 mL TPP tube. Then add 1 volume (~5mL) of phenol-chloroform: isoamyl alcohol (48:2) mix. Shake well to mix. Spin down for 15 min at 4000 rpm at 4°C, transfer upper phase (approximately 4 mL) to a new 15 mL TPP tube. Add 4 mL isopropanol to precipitate the nucleic acids, and leave it at −20°C for 25 min. After this, spin down at 5000rpm, 15 min at 4°C, remove all the solution, and completely dry the tube by keeping it up-side down on a tissue to remove all the liquid. Add 6 mL 4M lithium chloride (Merck, Cat. No. 1.05679) to resuspend the precipitate. The volume used depends on the size of the pellet. Shake until the pellet completely dissolves. Note that the pellet contains DNA along with the RNA. Leave on ice for 5 min, and spin down at 4500 rpm for 15 min at 4°C, remove all the solution and dry the tube completely. Add 7 mL 75% ethanol to resuspend the precipitate and leave it at room temperature for 10 min. Spin down at 4500 rpm for 15 min, remove all the solution and dry the tube completely with a tissue. A pellet will be visible if the amount of RNA is abundant. Add 75% ethanol and keep sample on ice or at −20°C for longer time. Repeat the 75% ethanol step once again. And dry the tubes at room temperature for 45min by keeping them open. Dissolve the RNA precipitation with ~700 μl DEPC treated water to a proper concentration. Dissolve RNA by gently pipetting. After a short spin, measure concentration and tRNA into a new 1.5mL tube. Store it under −80°C.

PolyA+ RNA purification

PolyA+ RNA was purified using magnetic Dynabeads Oligo(dT)25 (ThermoFisher, Cat. No. 61005). In brief, total RNA (75 μg) was adjusted to 100 μL with nuclease free water. The RNA was heated to 65°C for 2 min, and placed on ice, to disrupt secondary structures. 200 μL (1 mg) of Dynabeads were transferred to a microcentrifuge tube and washed twice with 100 μL Binding Buffer (1 M LiCl2, 2 mM EDTA, pH 8.0, 20 mM Tris-HCl, pH 7.5). Beads in 100 μL Binding Buffer were mixed with 100 μL of previously heated RNA. Beads were mixed thoroughly and rotated on a roller or mixer for 10 min at room temperature to allow the mRNAs to anneal to the oligo (dT)25 on the beads. Unbound fraction was discarded and beads were twice washed with 200 μL Washing buffer B. Washing buffer was removed and the elution was perform in the 20 μL of nuclease free water by heating at 80°C for 2 min, immediately placed on the magnet and the eluted PolyA+ RNA was transferred to a new RNase-free tube. For RNA mass spectrometry experiments, we repeated polyA + purification for a total of three times. The eluted RNA from the previous round was diluted to 100 μL in binding buffer for subsequent second or third round of purification. Used beads were washed twice in Wash buffer. After their resuspension in 100 μL of Binding Buffer, the purification was repeated as in the first round of purification.

Quantification of RNA modifications using LC-MS/MS

RNA was hydrolyzed to ribonucleosides by 20 U benzonase (Santa Cruz Biotech) and 0.2 U nuclease P1 (Sigma) in 10 mM ammonium acetate pH 6.0 and 1 mM magnesium chloride at 40°C for 1 h. After that, ammonium bicarbonate to 50 mM, 0.05 U phosphodiesterase I and 0.1 U alkaline phosphatase (Sigma) were added, and incubated further at 37°C for 1 h. Digested samples were precipitated with 3 volumes of acetonitrile, centrifuged (16,000xg, 30 min, 4°C), and supernatants were lyophilized and dissolved in a solution of stable isotope labeled internal standards for LC-MS/MS analysis. Chromatographic separation was performed using an Agilent 1290 Infinity II UHPLC system with an ZORBAX RRHD Eclipse Plus C18 150 × 2.1 mm ID (1.8 μm) column protected with an ZORBAX RRHD Eclipse Plus C18 5 × 2.1 mm ID (1.8 μm) guard column (Agilent). The mobile phase consisted of A: water and B: methanol (both added 0.1% formic acid) at 0.22 mL/min, for modifications starting with 5% B for 0.5 min followed by 2.5 min of 5–15% B, 3.5 min of 15–95% B, and 4 min re-equilibration with 5% B. Unmodified nucleosides were chromatographed with a 4 min gradient of 5–95% B and 4 min re-equilibration with 5% B. Mass spectrometric detection was performed using an Agilent 6495 Triple Quadrupole system operating in positive electrospray ionization mode, monitoring the mass transitions 269.1-150.1 (m^6Am), 282.1-150.1 (m^6A), 282.1-136.1 (Am), 268.1 (A), 284.1-152.1 (G), 244.1-112.1 (C), 245.1-113.1 (U), 296.1-164.1 ($m^6{}_2A$), and 298.1-166.1 (m^7G), 285.1-153.1 (d_3-m6A), 301.1-152.1 (d_3-Gm), 273.1-136.1 ($^{13}C_5$-A), and 246.1-114.1 (d_2-C). The m^6Am modification is catalyzed by PCIF1.[11] It carries out the N^6 methylation (m^6A) of the transcription start site adenosine that is already methylated on the ribose (Am; cap1) by CMTR1. Therefore, we used m^6Am levels as a readout for reduction in cap1 levels in the conditions lacking CMTR1 activity (Figures 3J and S4B).

RNA library preparation and sequencing

Library preparation for embryos form the heterozygous (HET) *Cmtr1*$^{+/-}$ crosses (n = 4) was performed at the *Genomics Core Facility* (GeneCore, EMBL Heidelberg) using 50 ng (for E6.5 embryos) and 200 ng (for E7.5 embryos) of total RNA with stranded rRNAminus RNAseq protocol and sequenced on NextSeq 500, HI, 75SE (85SE).

Library preparation and sequencing of a second batch of embryos from the heterozygous (HET) *Cmtr1*$^{+/-}$ crosses or *Cmtr2*$^{+/-}$ crosses was performed at iGE3 facility at the University of Geneva. We used 50 ng (for E6.5 embryos) and 200 ng (for E7.5 embryos)

of total RNA for the Smarter Ribodepletion kit. The prepared libraries were sequenced on the Illumina HiSeq 4000 sequencer (iGE3 Genomics Platform, University of Geneva).

Libraries were prepared with total RNA (500 ng) from human HAP1 WT and *CMTR1* KO (n = 4) cells at the *Genomics Core Facility* (GeneCore, EMBL Heidelberg) sequencing facility using the stranded rRNAminus RNAseq protocol and sequenced on the HiSeq2000.

All sequencing libraries prepared are listed in Table S2.

Polysome and ribosome profiling

Mouse liver was isolated from biological duplicates of control and *Cmtr1* cKO animals described previously. The tissue was rapidly cut up into small pieces and snap frozen in liquid nitrogen.

For one sample of human HAP1 cells, three 10 cm plates of ~70% confluency were used. Cells were treated with 100 μg/mL cycloheximide (CHX) at 37°C, media was removed and the plate was placed on ice. Cells were washed with ice-cold PBS containing 100 μg/mL CHX and the PBS was completely removed. Cells were collected by scraping in 1mL of ice-cold PBS supplemented with 100 μg/mL CHX. Cells were collected in Eppendorf tubes on ice and spun down for 5 min at 1000 rpm (200xg), 4°C. Supernatant was discarded and cell pellet was flash-frozen and stored at −80°C. Human HAP1 cell pellets were flash-frozen until further use. The ribosome profiling[79,80] and polysome fractionation was performed at the ''BioCode: RNA to Proteins'' Core Facility, Faculty of Medicine, UNIGE.

Polysome gradient centrifugation

Mouse liver tissues or HAP1 cell pellets were mechanically disrupted in liquid nitrogen and homogenized in a lysis buffer (50 mM Tris, pH 7.4, 100 mM KCl, 1.5 mM MgCl2, 1.0% Triton X-100, 0.5% Na-Deoxycholate, 25 U/mL Turbo DNase I, 1mM DTT, 100 μg/mL cycloheximide, and Protease inhibitors (Roche). 10 μL of SUPERaseIn RNase inhibitor (Ambion, #AM2694) was added to lysis buffer upon homogenization. Cell debris were pelleted (20000xg, 20 min, 4°C). Approximately 500 μL of tissue lysates containing 2 μg/mL of total RNA (1000 μg of total RNA) were loaded on the linear 20–60% sucrose gradients prepared on the gradient buffer (50 mM Tris, pH 7.4, 100 mM KCl, 1.5 mM MgCl2, 1mM DTT, 100 μg/mL cycloheximide). Ribosomes were fractionated at 247′600xg (38′000 rpm, rotor SW41 Ti (Beckman Coulter, #331362) for 3 h 30 min at 4°C. Fractionated ribosomes were monitored and collected using Density Gradient Fractionation System (ISCO) (Figures 3K and S3D).

Ribosome profiling

Mouse liver tissues or HAP1 cell pellets were mechanically disrupted in liquid nitrogen and homogenized in a lysis buffer (50 mM Tris, pH 7.4, 100 mM KCl, 1.5 mM MgCl2, 1.0% Triton X-100, 0.5% Na-Deoxycholate, 25 U/mL Turbo DNase I, 1mM DTT, 100 μg/mL cycloheximide, and Protease inhibitors (Roche, Cat. No. 04693132001). For determination of the optimal concentration of nuclease for RNA digestion, the extracts were treated with the different amounts of RNAse I (Ambion, #AM2295). This was followed by sucrose gradient centrifugation to determine shift of polysomes to monosomes, but without further degradation of monosomes.

To obtain ribosome footprints, 0.12 mL of total extracts containing 300 μg of total RNA were treated with RNAse I (Ambion, #AM2295) (250U/1 mg of total RNA), for 45 min at 20°C with slow agitation. 10 μL SUPERaseIn RNase inhibitor (Ambion, #AM2694) was added to stop nuclease digestion. Monosomes were isolated using MicroSpin S-400 HR spin columns (Amersham, #27514001). For isolation of ribosome protected mRNA fragments (RPF), 3× volumes of QIAzol (Qiagen, Cat. No. 79306) were added to the S-400 eluate, mixed thoroughly, and RNA extracted with Direct-Zol RNA Mini Prep Plus kit (Zymo Research, #R2070).

Ribosome protected fragment (RPF) library preparation

Libraries were prepared as described.[79,80] Briefly, ribosome protected fragments (RPFs) were size-selected (25–34 nt) by electrophoresis using a 15% TBE-Urea polyacrylamide gel electrophoresis (PAGE) and two RNA markers, 25-mer (OP-RNA25) and 34-mer (OP-RNA34) (Table S1). After dephosphorylation with T4 Polynucleotide Kinase (NEB, #M0201S) the adapter Linker-1 (OP-RNA45) was ligated to the 3′ end of the RPF using T4 RNA Ligase 2 (NEB, #M0242S). The ligated products were purified using 10% TBE-Urea PAGE. Ribosomal RNA was removed using RiboCop rRNA Depletion Kit V2 H/M/R (Lexogen #144) for mouse liver samples or using the Ribo-Zero Plus rRNA Depletion kit (Illumina, #20040892) for HAP1 cell samples. The adapter Linker-1 was used for priming reverse transcription (RT) with the RT primer Ni-Ni-9 (OP27) using ProtoScript II Reverse Transcriptase (NEB, #M0368S). RT products were purified using 10% TBE-Urea PAGE. The cDNA was circularized with CircLigase II ssDNA Ligase (Epicentre, #CL9021K). The final libraries were generated by PCR using forward index primer NI-N-2 (OP28) and reverse index primers. Amplified libraries were purified using 8% TBE-PAGE and analyzed with TapeStation. Libraries were sequenced on an Illumina HiSeq 4000, single-reads, 1 × 50 bp, 8 libraries in a pool.

Isolation of total RNA, library preparation and sequencing

Total RNA was isolated from the same nuclease-treated extracts, that were used to obtain RPFs, using Direct-Zol RNA Mini Prep Plus kit (Zymo Research, #R2070). RNA was sent to iGE3 Genomic Platform, University of Geneva for stranded mRNA library preparation. Libraries were sequenced on an Illumina HiSeq 4000, single-end reads, 1 × 50 bp, 12 libraries in pool.

All sequencing libraries prepared are listed in Table S2.

QUANTIFICATION AND STATISTICAL ANALYSIS

Analysis of RNA-seq data

Quality control of the demultiplexed libraries was performed with FastQC.[63] Sequencing adapters were removed by Flexbar software.[64] All the sequenced mouse libraries were aligned to the mouse transcriptome (GRCm38 assembly) with STAR[65] (v2.7.10a) and reads were further quantified transcript-wise from STAR-generated BAM files by salmon quant (v1.8.0)[62] with the following options: –seqBias –gcBias –posBias –writeUnmappedNames. Transcript counts were collapsed into gene counts and DESeq function of the DESeq2 bioconductor package[60,61] was used to obtain log2 fold changes of gene expression between control and mutant samples and the adjusted p values. Hidden noise was inferred by the sva bioconductor package[75] and 2 surrogate variables (SV1 and SV2) were included into DESeq function model (design = ~ SV1 + SV2 + condition). Adjusted p value 0.05, as well as the absolute value of log2 fold change 1 were defined as thresholds of statistical significance. All the visualizations were done in Python 3.10.6. Volcano plots of differential gene expression was plotted using scatterplot function of the seaborn (v0.12.1) package[66] with additional matplotlib (v3.6.2) customizations[67] (Table S3). Boxplots of the expression of immune sensors (Figure 1F), comparison of the alternative splicing events (Figure 1G), z-scores of the log2-transformed counts of the snoRNA-containing introns (Figure S1F), log2 fold changes of selected gene classes expression and translational efficiency (Figure S1G, S3F–S3G, and S4F), as well as follicle proportions (Figure S2D) were plotted with the boxplot function of the seaborn package. Stacked bar charts of embryo genotypes (Figures 1C and 4C), and bulk-to-single-cell projections (Figure S1E and S5H) were created with the plot function (kind = 'bar', stacked = True) from the pandas (v1.5.1) package. Heat maps of the type I IFN pathway genes (Figure 3G) and selected innate immune sensors across early embryonic stages (Figure S1D) were plotted with clustermap function with z_score and weighted hierarchical clustering options of the seaborn package. The early embryonic transcriptome data used for analysis in Figure 1F was from published sources (GEO: GSE45719 and GSE119945; Arrayexpress: E-MTAB-6967). Venn diagrams comparing *Cmtr1* and *Cmtr2* dysregulated gene sets in E6.5 and E7.5 embryos (Figure 4F) were plotted with venn2 function of the matplotlib_venn (v0.11.7) package. Genes found to be significantly up- or down-regulated in the mutants were searched for enriched Gene Ontology terms in the Biological Process and Molecular Function ontologies using ENRICHR[58] and plotted with barplot function of the gseapy (v0.14.0) package.[68] Violin plot comparing expression levels of RIG-I between HAP1 cells and control *Cmtr1* mice (Figure S4G) was plotted by violinplot function of the seaborn (v0.12.1) package.

Analysis of ribosome profiling data

Quality control of the demultiplexed libraries was performed with FastQC.[63] Sequencing adapters were trimmed with Flexbar.[64] Ribosomal RNA filtering was done by aligning reads to the rRNA index with bowtie[69] with the following options: -S -v 1 -a –best –strata. After rRNA filtering step remaining pool of reads was aligned to a relevant genome: GRCm38 assembly for the mouse liver data and the GRCh38 assembly for human HAP1 cells, respectively. Genome alignment was performed by STAR[65] without any further read clipping by adding –alignEndsType EndToEnd option. Read coverage biases were checked from the BAM files by the CollectRnaSeqMetrics program from "Picard Toolkit".[70] Metagene profile analysis of the read phasing of the mouse liver data (Figure S3E) was performed by metagene program from the plastid python package.[76] RiboCode toolkit[71] was used to detect longest translated ORFs (-l yes). Count tables of the longest translated ORFs for further differential translation efficiency analysis were made by ORFcount program from the RiboCode toolkit. First and last 10 translated codons were masked from counting (-f 10 -L 10). Hidden noise was inferred by sva bioconductor package[75] and 2 surrogate variables (SV1 and SV2) were included into model. Differential translational efficiency analysis was done by DESeq function from DESeq2 bioconductor package with the following parameters specified: test = "LRT", reduced = ~SV1 + SV2 + assay + condition. Model design was as follows: ~SV1 + SV2 + assay + condition + assay:condition. Volcano plots showing differential translational efficiency (Table S4) between mouse *Cmtr1* cKO (*Cmtr1*$^{-/loxP}$; Alb-CreERT$^{+/-}$) and control (*Cmtr1*$^{+/loxP}$; AlbCreERT$^{+/-}$) (Figure 3L), as well as between human HAP1 *CMTR1* KO and WT cells (Figure S4F) were plotted using scatterplot function of the seaborn (v0.12.1) package with additional matplotlib (v3.6.2) customizations. Coverage tracks comparing ribosome protected fragments (RPFs) and input read distributions across gene model (Figure 3M) were plotted by SparK (v2.6.2) python library.[72]

Analysis of alternative splicing events

The annotation file of the alternative splicing (AS) events (SE – skipped exon, MX – mutually exclusive exons, A5/3 – alternative 5′/3′ site, RI – retained intron, AF – alternative first exon, AL – alternative last exon) was generated by generateEvents script from the SUPPA2 toolkit.[73] All the AS events were filtered based on the total gene expression counts (total TPM counts per gene per all conditions >10). The PSI (Percent Spliced-In) scores (Figure 1G) representing proportions of reads supporting the event over total amount of reads per gene were computed by psiPerEvent script from the SUPPA2 toolkit both per all the retained AS events and per transcripts (percentage of reads supporting a specific AS event over total number of events per gene, and percentage of reads supporting a specific transcript over total amount of reads per gene, respectively). Cryptic and/or rare AS events with PSI scores <0.05 or >0.95 as well as events with <25% of missing values per event were filtered out from further

analysis. The remaining missing values were imputed from the 2 neighbors by the KNN algorithm (KNNImputer function) from the sklearn library package (v1.1.3).[77]

Bulk-to-single-cell deconvolution (RNA-seq debulking)

All the bulk-to-single-cell deconvolutions of the E6.5 and E7.5 *Cmtr1* and *Cmtr2* knock-out samples were performed with SCDC (v0.0.0.9000) R package[74] on the published single-cell embryonic atlases.[81]